doi.org/10.1002/cssc.202002098

Chemistry Europe
European Chemical Societies Publishing

Single-Atom and Dual-Atom Electrocatalysts Derived from Metal Organic Frameworks: Current Progress and Perspectives

Siru Chen[+],*[a] Ming Cui[+],[b] Zehao Yin,[b] Jiabin Xiong,[a] Liwei Mi,*[a] and Yanqiang Li*[b]

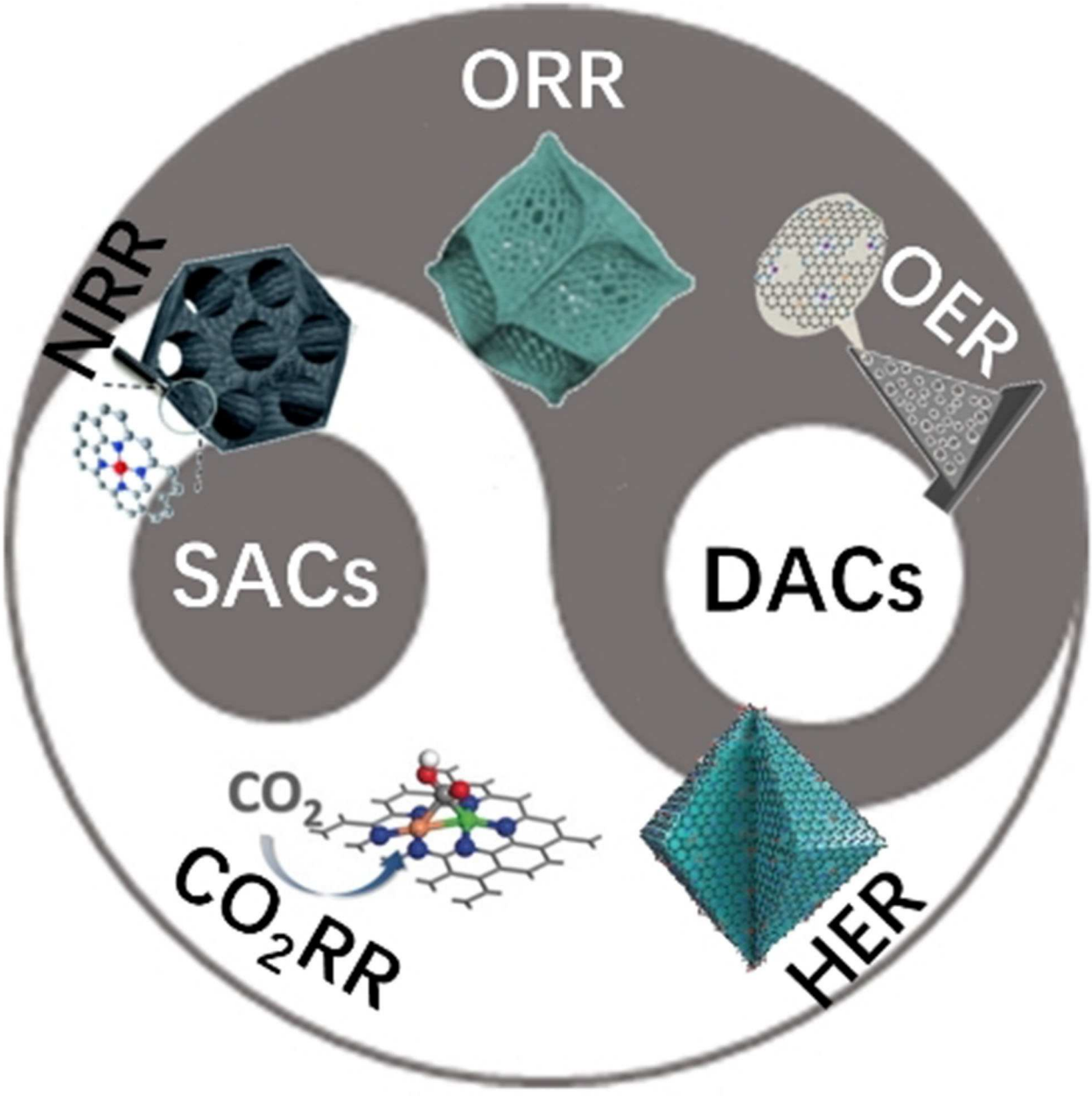

Single-atom catalysts (SACs) have attracted increasing research interests owing to their unique electronic structures, quantum size effects and maximum utilization rate of atoms. Metal organic frameworks (MOFs) are good candidates to prepare SACs owing to the atomically dispersed metal nodes in MOFs and abundant N and C species to stabilize the single atoms. In addition, the distance of adjacent metal atoms can be turned by adjusting the size of ligands and adding volatile metal centers to promote the formation of isolated metal atoms. Moreover, the diverse metal centers in MOFs can promote the preparation of dual-atom catalysts (DACs) to improve the metal loading and optimize the electronic structures of the catalysts. The applications of MOFs derived SACs and DACs for electrocatalysis, including oxygen reduction reaction, oxygen evolution reaction, hydrogen evolution reaction, carbon dioxide reduction reaction and nitrogen reduction reaction are systematically summarized in this Review. The corresponding synthesis strategies, atomic structures and electrocatalytic performances of the catalysts are discussed to provide a deep understanding of MOFs-based atomic electrocatalysts. The catalytic mechanisms of the catalysts are presented, and the crucial challenges and perspectives are proposed to promote further design and applications of atomic electrocatalysts.

1. Introduction

The depletion of fossil fuels and ever-increasing demands for energy prompt scientists to develop advanced energy conversion techniques. The fuel cells, metal–air batteries, and water electrolyzers are several promising energy conversion devices owing to their high efficiencies and environmentally friendly characters.[1–3] Oxygen reduction reaction (ORR), oxygen evolution reaction (OER) and hydrogen evolution reaction (HER) are the core reactions in these devices and the kinetics of the reactions determine the energy conversion efficiency of these devices to a great extent.[4–6] Therefore, the development of corresponding electrocatalysts to reduce the energy barrier and facilitate kinetics of electrochemical reactions is an effective strategy to increase the efficiency of the above energy conversion devices. In addition, fossil fuels are still the main source of energy in contemporary society, and the burning of fossil fuels causes serious environmental issues such as greenhouse effect owing to the emissions of CO_2. Therefore, developing proper technologies to reduce the amount of CO_2 in the atmosphere is necessary.[7–9] Electrocatalytic CO_2 reduction reaction (CO_2RR) is a method to kill two birds with one stone, for it not only can effectively reduce the amount of CO_2, but also can converse CO_2 into useful chemicals and fuels such as methanol, formic acid and hydrocarbons.[10–12] However, this technology suffers from the poor product selectivity and low faradic efficiency. Therefore, designing proper electrocatalysts to improve the faradic efficiency and product selectivity is very important. Moreover, NH_3 is one of the most important chemicals and carbon-free energy carriers. At present, NH_3 is primarily produced through Haber-Bosch process at high-temperatures and high-pressures (200–300 atm, 400–550 °C) using iron- or ruthenium-based catalysts. However, this process takes up 1% total fossil energy and emits more than 450 million tons of carbon dioxide each year, posing a major threat to sustainable energy development and environmental protection.[13–15] Fortunately, the electrocatalytic nitrogen reduction reaction (NRR) can produce NH_3 at ambient conditions using renewable energy, and the investigation of NRR catalysts to improve the NRR yields and faradic efficiency is also very significant.[16–18]

Electrocatalysts based on precious metals usually show outstanding catalytic performance owing to the high intrinsic catalytic activity induced by their electronic structures. For example, noble metal Pt is the best electrocatalysts toward HER and ORR, while IrO_2 and RuO_2 are considered as outstanding electrocatalyst for OER.[19–21] However, the low reserve, high cost, and poor stability of precious metals catalysts limit their commercial applications. Therefore, the investigation of high efficiency, low cost and stable noble metal-free electrocatalysts is imperatively meaningful and transition metal-based catalysts emerged owing to their moderate catalytic activity and tunable electronic structures to optimize the adsorption of intermediates during the reaction process.[22–26]

Reducing the content of metals is a valid method to reduce the cost of transition metal-based electrocatalysts. In order to maintain the high activity of catalysts when the loading of metal is decreased, it is necessary to improve the utilization rate of metal atoms. The utilization rate of metal atoms can be improved by reducing the size of metals to create more metal sites. Generally, the utilization rate of metal atoms reaches the maximization when the size of metals is decreased to a single atom.[27–29] In addition, the quantum size effects and interactions between the single metal atom and the supports in the single-atom catalysts (SACs) not only can further boost the catalytic activity, but also can achieve outstanding stability owing to the uneasy aggregation of single atoms confined by the supports.[30,31] Moreover, the catalytic performance derived from SACs is more approximate to the theoretical calculation results, where an atomic structure theoretical model must be established when conducting the theoretical calculations.[32,33] Therefore, SACs are also good candidates for investigation of reaction mechanisms and identification of active sites.

Traditionally, SACs can be prepared from wet-impregnation method, coprecipitation method, successive reduction method

[a] Dr. S. Chen,[+] Dr. J. Xiong, Prof. L. Mi
Henan Key Laboratory of Functional Salt Materials
Center for Advanced Materials Research
Zhongyuan University of Technology
Zhengzhou, 450007 (P. R. China)
E-mail: siruchen@zut.edu.cn
mlwzzu@163.com
[b] M. Cui,[+] Z. Yin, Dr. Y. Li
State Key Laboratory of Fine Chemicals
School of Petroleum and Chemical Engineering
Dalian University of Technology
Panjin Campus, Panjin 124221 (P. R. China)
E-mail: yanqiangli@dlut.edu.cn
[+] These authors contributed equally to this work.

and spatial confinement strategy.[34–39] Recent research demonstrated that metal organic frameworks (MOFs) are good precursors for synthesizing SACs owing to the following reasons. Firstly, the metal nodes in MOFs are atomically dispersed and stabilized by organic ligands, which make its more readily to avoid the aggregation of metal atoms upon pyrolysis.[40,41] Secondly, the organic ligands in MOFs can be converted into highly porous carbons in the thermal annealing process. The carbons can not only serve as supports to stabilize metal single atoms, but also can provide extra active sites and facilitate electrons and ions transport during the catalytic reactions. Thirdly, the regular morphology of MOFs can be inherited during the pyrolysis process, which make it possible to design MOFs with desirable morphology to prepare SACs with more exposed edges or surfaces for catalysis. Fourthly, by precisely designing and tailoring the structures and components of MOFs, it is convenient to realize coordination environment regulation of SACs based on MOFs. Moreover, the various metal centers in MOFs can also promote the preparation of dual-atom catalysts (DACs), where the metal atoms loading can be increased and the electronic structures of the catalysts can be adjusted by the introduction of dual metal active sites to break the linear relationship between the adsorption energies of reaction intermediates, further improving the catalytic performance of the catalysts.[42,43]

Considering the ever-increasing atomic catalysts and MOFs based catalysts for electrocatalysis, a specific review focused on SACs and DACs derived from MOFs is important for readers to get a systematically understanding in this field, although some other reviews have discussed this partially.[44–47] In this review, we summarize the recent progress and development of SACs and DACs from MOFs for electrocatalytic applications including ORR, OER, HRR, CO_2RR and NRR (Figure 1). This review aims to give readers a deep understanding of atomic electrocatalysts derived from MOFs and promote the development of MOFs derived atomic electrocatalysts. The synthesis-structure-property correlations of the catalysts are discussed in detail and several important milestones are highlighted. In addition, the main challenges and perspectives are proposed for further design and applications of MOF-based atomic electrocatalysts.

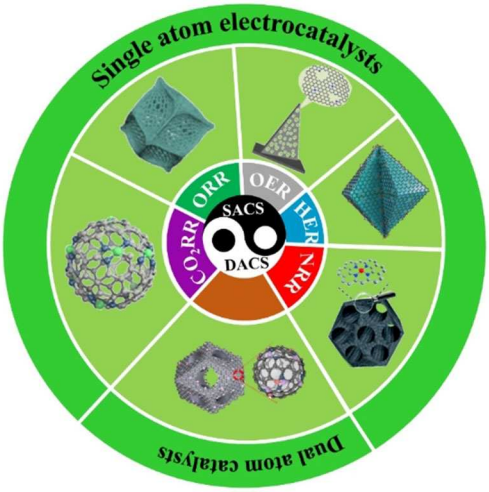

Figure 1. Organization of the main contents in this review. (ORR image: Reproduced with permission.[70] Copyright 2020, Wiley-VCH; OER image: Reproduced with permission.[92] Copyright 2018, American Chemistry Society; HER image. Reproduced with permission.[101] Copyright 2018, Wiley-VCH; CO_2RR image: Copyright 2017, American Chemistry Society. Reproduced with permission.[51] NRR image. Copyright 2019, Royal Society of Chemistry. Reproduced with permission.[115] DAC image. Reproduced with permission.[125] Copyright 2017, American Chemistry Society.)

2. Single-atom Electrocatalysts Derived from MOFs

The concept of SACs was firstly proposed by Zhang and coworkers in 2011, where single atom Pt catalysts loading on the surface of FeO_x was prepared through coprecipitation method.[48] Later in 2016, atomically dispersed nickel species

Dr. Siru Chen received her Ph.D. degree at Jilin University in 2015. After three years research in Dalian Institute of Chemical Physics as a post-doctor, she joined Zhongyuan University of Technology as a lecturer in 2019. Her research focuses on the design and preparation of functional materials and catalysts for electrochemical energy storage and conversion.

Ming Cui is a Master's degree candidate at Dalian University of Technology. He received his bachelor's degree from Liaocheng University. His research focuses on designing bifunctional electrocatalysts for high-performance zinc-air batteries.

Liwei Mi received his B.S., M.S. and Ph.D. from Zhengzhou University. In 2014, he worked as a professor of materials science in Zhongyuan University of Technology. His current research interest focuses on the controllable preparation and performance study of functionalized micro/nanomaterials.

Yanqiang Li received his Ph.D. degree from state key laboratory of inorganic synthesis & preparation chemistry Jilin University in 2015. Then, he joined Dalian University of Technology as a lecturer. His research focuses on the design and preparation of functional materials and catalysts for electrochemical energy storage and conversion based on the combination of theoretical studies and electrochemical experiments.

supported by graphitized carbon were developed for HER and atomically isolated Co in N-doped carbon for ORR were prepared form MOFs.[49,50] In 2017, Li and co-workers developed Ni-based SACs for CO_2RR and Zeng and co-workers reported Ru single atoms for NRR using MOFs as precursors.[51,52] In addition, DACs with high performance for ORR and CO_2RR were also reported and rapid progress were achieved in MOFs derived atomic catalysts for electrocatalysis (Table 1 and Table 2).

Table 1. Some representative SACs derived from MOFs for ORR and DACs electrocatalysis.

Catalyst	Precursor	Synthetic method	Major advance and significance	$E_{1/2}$[a] [V]y	Ref.
Fe SAs–NC	FePc@ZIF-8	pyrolysis acid leaching	selective C–N bond cleavage to tailor the coordination environment of pyridinic N to achieve edge-site engineering of Fe–N_4 moieties	0.915	[65]
3DOM Fe–N-C	PS@ZIF-8 ferrocene	pyrolysis	templating method to prepare hierarchical ordered porous with atomic Fe–N–C sites	0.875	[69]
Fe/OES	Fe/ZIF-8@SiO_x	pyrolysis acid leaching	overhang-eave carbon cages with edge-rich structure to expose more active sites at three-phase boundaries	0.85	[70]
Fe–SAs/NPS–HC	ZIF-8/Fe@PZS	pyrolysis	P and S dopants could reduce the positive charge of Fe in Fe–N_4–C to weaken the binding of OH species	0.912	[71]
Co SAs/N–C	ZnCo-ZIF	pyrolysis	Co–N_4 and Co–N_2 active sites for ORR	0.881	[50]
Co–N–C@F127	Co-ZIF-8@F127	pyrolysis	CoN_{2+2} moiety with lower activation energy for the dissociation of OOH	0.84	[82]
Cu–SAs/N–C	Cu foam ZIF-8	direct atoms[b]	large-scale synthesis of SACs from bulk metals	0.895	[85]
Co–N–C-10	ZnCo-ZIF	pyrolysis	Co_2N_5 site exhibited reduced thermodynamic barrier for ORR	0.79[c]	[123]
CoPNi–N/C	ZIF-67 on Ni-complex	pyrolysis	synergetic effect of Co/Ni–N–C bonds	0.84	[124]
(Fe, Co)/N–C	$FeCl_3$/ZnCo-ZIF-8	pyrolysis	(Fe, Co)/N–C could decrease the cleavage barrier of O–O bond to favor four electron ORR pathway	0.954	[126]

[a] In 0.1 M KOH; [b] emitting from bulk metals with ammonia; [c] in 0.1 M $HClO_4$.

Table 2. Some representative SACs derived from MOFs for OER, HER, CO_2RR and NRR..

Catalyst	Precursor	Synthetic method	Application	Major advance and significance	Activity	Ref.
CUMSs-ZIF-67	ZIF-67	dielectric barrier discharge plasma etching	OER	coordinative unsaturated metal sites (CUMSs) created by N_2 plasma	$\eta = 410$ mV @ 10 mA cm^{-2} in 0.5 M KBi	[90]
CoO_x–ZIF	ZIF-67	O_2 plasma treatment	OER	CoO_x active sites created by O_2 plasma	$\eta = 318$ mV @ 10 mA cm^{-2} in 1 M KOH	[91]
NC-CoSA	ZIF-67	pyrolysis and acid leaching	OER	self-supporting SACs on carbon for binder and additives-free Zn-air batteries	$\eta = 360$ mV @ 10 mA cm^{-2} in 0.1 M KOH	[92]
A–Ni-C	Ni-MIF	pyrolysis and acid leaching	HER	In-site generated Ni single atoms via electrochemical activation	$\eta = 34$ mV @ 10 mA cm^{-2} in 0.5 M H_2SO_4	[49]
Co–SAC	ZnCo-biMOF	pyrolysis and acid leaching	HER	DMOSO guest molecular assist the preparation of SACs	$\eta = 260$ mV @ 10 mA cm^{-2} in 0.5 M H_2SO_4	[97]
W-SAC	WCl_5/UiO-66-NH_2	pyrolysis and acid leaching	HER	$W_1N_1C_3$ exhibited smaller ΔG_{H^*} than WC and WN	$\eta = 85$ mV @ 10 mA cm^{-2} in 0.1 M KOH	[101]
Co SACs	Co/Zn ZIF	pyrolysis	CO_2RR	Co–N_4 < Co–N_3 < Co–N_2, a low coordination number could promote the activation of CO_2 to CO_2^- intermediate	94% CO FE, $\eta = 520$ mV in 0.5 M $KHCO_3$	[105]
Ni_{SA}–N_x–C	MgNi-MOF-74	pyrolysis and MgO removal	CO_2RR	Ni_{SA}–N_2–C > Ni_{SA}–N_3–C > Ni_{SA}–N_4–C, Ni_{SA}–N_2–C exhibited much lower ΔG for formation of COOH*	98% CO FE at −0.8 V in 0.5 M $KHCO_3$	[106]
Fe–N–C	Fe/ZIF-8	pyrolysis	CO_2RR	Fe–N_{2+2}–C_8 is more active than Fe–N_4-C	93% CO FE, $\eta = 470$ mV in 0.5 M $KHCO_3$	[107]
Bi SAs/NC	Bi-MOF	pyrolysis	CO_2RR	Bi-N_4 moieties had a lower free energy for the formation of COOH*	97% CO FE at −0.5 V in 0.1 M $NaHCO_3$	[109]
Fe_1–N–C	PCN-222(Fe)	pyrolysis and acid leaching	NRR	Mixed ligands strategy, Fe_1–N–C low Gibbs free energy for N_2* to N_2H*, and more positive charge to suppress HER	NH_3 yield: 1.56×10^{-11} mol cm^{-2} s^{-1} at −0.05 V	[115]
Ru SAs/N–C	Ru(acac)$_3$/ZIF-8	pyrolysis	NRR	Ru_1–N_3 had a smaller ΔG of N_2 dissociation than Ru (101)	NH_3 yield: 120.9 μg mg^{-1} h^{-1} in 0.05 M H_2SO_4	[52]

2.1. SACs derived from MOFs for ORR

ORR is a very critical reaction in metal–air batteries and fuel cells. Generally, the ORR process is divided into a two-electron ($2e^-$) transport pathway and a four-electron ($4e^-$) transport pathway according to different types of oxygen adsorption on the surface of catalysts. Among them, the end-on O_2 adsorption mode promotes the $2e^-$ pathway; the bidentate O_2 adsorption mode promotes the $4e^-$ pathway. However, in the $2e^-$ route, corrosive peroxides are generated, which is harmful to the stability of the batteries.[53,54] Therefore, in practical battery applications, catalysts that could promote ORR through the direct $4e^-$ reduction pathway is particularly desirable.

There are lots of oxygen-containing intermediates during ORR, such as OOH*, O* and OH*. The key to improve the ORR reaction kinetics is to effectively control the adsorption energy of these intermediates.[55,56] Since the rate determination steps ORR on different catalysts are different, it is necessary to reasonably adjust the electronic structure of catalysts to optimize the adsorption energy of intermediates, thereby reducing the overpotential of the catalyst and achieving rapid ORR kinetics. When the size of metal active sites is reduced to single atoms, the electronic structure of the metal atoms is different with that in bulk owing to the low-coordinated configuration of the SACs, therefore SACs are very promising for ORR.

Fe-based SACs is the most extensively investigated catalysts toward ORR owing to the intrinsic high catalytic activity of Fe atoms.[57–62] Xu and coworkers used MIL-101-NH_2 with mesopores of 2–3 nm to accommodate $FeCl_3$ and dicyandiamide, which served as Fe sources and N dopants after pyrolyzing.[63] Atomically dispersed FeN_x species with high catalytic activity toward ORR were obtained on N-doped carbons and the catalyst exhibited hierarchical pore structures for rapid mass transport. As a result, the catalyst displayed outstanding ORR performance with half-wave potential ($E_{1/2}$) is even higher than commercial 20 wt% Pt/C catalyst.

ZIF-8 is a good precursor to prepare SACs owing to its N-containing ligands, regular morphology and readily preparation at ambient temperatures.[64–71] Using Fe-doped ZIF-8 as precursors, Wu and co-workers prepared atomically dispersed Fe in N-doped carbons for ORR. In addition, the size of ZIF-8 was systematically adjusted from 20 to 1000 nm to investigate the size effect of carbon supports.[64] The active sites were demonstrated to be FeN_4 moieties and the best ORR performance were obtained when the size of carbon was 50 nm.

Encapsulating Fe-containing organic salts into ZIF-8 is also a good strategy to prepare Fe SACs. In a recent work, iron(II) phthalocyanine (FePc), whose molecular size is even larger than the cavity of ZIF-8 cage was introduced during the synthesis process of ZIF-8 to prepare isolated Fe–N_4 sites in N-doped carbon (Figure 2A).[65] The usage of FePc could break the

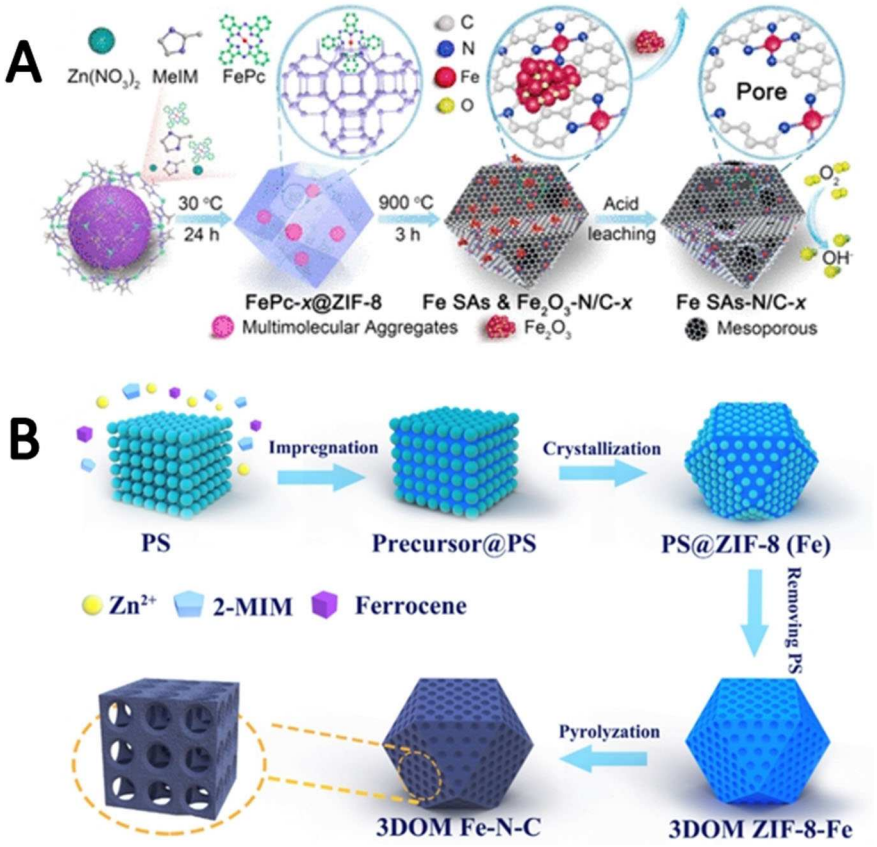

Figure 2. (A) Diagram for the synthesis route of Fe SAs-N–C. Reproduced with permission.[65] Copyright 2018, American Chemical Society. (B) Schematic illustration for the synthesis of 3DOM Fe–N–C. Reproduced with permission.[69] Copyright 2020, Elsevier.

confinement effect of microcavity and bursted some C–N bonds neighboring Fe–N_4 sites to realize edge-site engineering of Fe–N_4. All the catalysts obtained by adding FePc exhibited higher ORR catalytic activity than Pt/C, demonstrating the advantages of the edge-hosted Fe–N_4 sites. Density functional theory (DFT) calculation indicated that the edge-hosted Fe–N_4 sites could tailor the bonding configuration of N and reduce the overall ORR barriers. Deng et al. introduced Ferrocene into the cage of ZIF-8 by evaporation method and high-density Fe–N_4 active sites dispersed in N-doped carbon atomically were prepared after pyrolyzing.[66] The optimized catalysts also show high ORR catalytic activity, with a high half-wave potential of 0.864 V in 0.1 M KOH. $Fe(acac)_3$ molecule was introduced into the cage of ZIF-8 by Li and co-workers to prepare single atom Fe in N-doped carbon (Fe-ISAs/CN) for ORR.[67] The aberration-corrected high-angle annular darkfield scanning transmission electron microscope (HAADF-STEM) image demonstrated the atomically dispersed Fe even when the Fe loading is up to 2.16 wt%. DFT calculations indicated that the ORR overpotential for Fe-ISAs/CN (0.65 V) is much lower than that for Fe particles (1.76 V). As a result, the half-wave potential of Fe-ISAs/CN was 60 mV higher than that of Pt/C catalyst. Coincidentally, Li et. al also used $Fe(acac)_3$ as Fe source in ZIF-8 to prepare Fe–N_x–C catalysts for ORR.[68] Moreover, they also used melamine to encapsulate ZIF-8 to extend the porosity of the prepared catalysts. Eventually, 3D hierarchical carbon with isolated Fe–N_x sites were obtained, which possessed the advantages of high catalytic active sites and rapid mass transport, showing outstanding ORR performance in both alkaline and acidic electrolyte. In another work, using Zn–Fe bimetallic ZIF as precursors, Zhu and co-workers prepared atomically dispersed Fe–N_x active sites embedded in mesoporous carbon nanoframes (CNF). The authors pointed out that the proper amount of Fe^{2+} dopants in ZnFe-ZIFs can accelerate the decomposition of metal-ligand linkages nearby and therefore forcing the generation of voids inside the derived carbon matrix during the pyrolysis process. The FeSAs/CNF-900 exhibited substantial multi-level pores in the range of 1–15 nm and high active Fe–N_x sites, which make its ORR performance much superior than that of 20 wt% Pt/C.[57]

The porosity of ZIF-8 derived SACs can also be extended by using extra template. In a recent work, ordered 3D PS assembly was used as a hard template during the formation of ZIF-8, and ferrocene was used as extra Fe source (Figure 2B).[69] After removing the PS template and sequent pyrolyzing, 3D hierarchically ordered porous with isolated FeN_4 sites (3DOM Fe–N–C) was prepared. Owing to the highly active isolated dispersed FeN_4 and enhanced kinetics induced by the 3D hierarchical structure, the 3DOM Fe–N–C-900 exhibits a high half-wave potential of 0.875 V in 0.1 M KOH. In addition, as an ORR catalyst for ZABs, a peak power density of 235 mW cm^{-2} and a specific capacity of 768.3 mAh g_{Zn}^{-1} were achieved.

Optimizing the morphology of an electrocatalyst to enable utmost exposed active sites and fast mass transport is also very attractive. Xu and co-workers developed a silica-mediated MOF-templated strategy to prepare overhang-eave structure (OES) carbon cage decorated with Fe single-atom (Fe/OES; Figure 3A).[70] Thanks to the edge-rich structure with more three-phase boundaries induced by its unique morphology, and the highly active Fe–N_4–C sites, the Fe/OES exhibited superior ORR performance than Pt/C both in 0.1 M KOH and 0.5 M H_2SO_4. In addition, the ZABs catalyzed by Fe/OES could achieve a capacity of 807.5 mAh g_{Zn}^{-1} and a peak power density of 186.8 mW cm^{-2}, demonstrating the practical applications of the catalyst.

As stated above, most of the reported carbon supported Fe-based SACs are based on N-doped carbon. Doping multiple heteroatoms into carbon can further modify the electronic configuration of the carbon, thereby boosting catalytic performance further. By coating poly(cyclotriphospazene-co-4,4′-sulfonyldiphenol; PZS) onto ZIF-8 as well as introducing Fe^{3+} in ZIF-8, Li and co-workers reported Fe single atoms imbedded in N, P, S tri-doped hollow carbon (Fe-SAs/NPS-HC) for ORR (Figure 3B).[71] The PZS coating not only leaded to P and S dopants, but also induced the hollow structure through Kirkendall effect. Though extended X-ray absorption fine structure (EXAFS) indicated that Fe atoms were only coordinated by N atoms, however, the DFT calculations exhibited that the S and P atoms around Fe–N_4 sites could denote electrons to Fe atoms, which could decrease the positive charge of Fe–N_4 and therefore weaken the binding of adsorbed OH species. As a result, the half-wave potential of Fe–SAs/NPS–HC (0.912 V) was much higher than that of Pt/C (0.84 V), and the Fe-SAs/NPS-HC could effectively drive the ORR in hydrogen-air fuel cells and zinc-air batteries.

Besides ZIF-8, many other MOFs are also be demonstrated as proper precursors to prepare SACs.[72,73] For example, using a porphyrinic MOF, PCN-222 with constructed by mixed ligands, Jiang and co-workers reported single atomic Fe anchored on N-doped carbon (Fe_{SA}–N–C; Figure 4A).[72] The dual ligands strategy could effectively control the distance of adjacent Fe in the MOF by varying the ration of the two ligands. As shown in Figure 4B and 4 C, the obtained Fe_{SA}–N–C were rod-like morphology and the Fe are atomically dispersed in the catalyst when the amount of Fe–TCPP [TCPP = tetrakis (4-carboxyphenyl) porphyrin] during the synthesis is 20% mol ratio versus H_2–TCPP. The Fe loading was estimated to be up to 1.76 wt% and all the Fe atoms were coordinated by four N atoms in the form of FeN_4 moiety (Figure 4D). The Fe_{SA}-N–C exhibited high catalytic activity toward ORR, as indicated by the LSV curves (Figure 4E). Coincidentally, by introducing polyaniline (PANI) into PCN-224(Fe), Cao and co-workers developed a migration-prevention strategy to prepare single-atom Fe anchored on N-doped carbon.[73] The PANI not only protect the Fe atoms from aggregation, but also served as N source to form Fe–N_x–C species. The Fe-based SACs also exhibited outstanding catalytic performance both in alkaline and acidic electrolyte.

Besides Fe atoms, Co also exhibited high ORR performance as indicated by Co based non-single atom catalysts.[74–77] Therefore, Co-based SACs were also developed to further improve the utilization rate of Co atoms and their catalytic activity. The single Co atoms derived from MOFs for ORR was firstly examined by Li and co-workers.[50] A ZnCo mixed-metal MOF was used as a precursor (Figure 5A). The evaporation of Zn at high temperatures played a critical role for the formation of Co single atoms, for it not only extend the spatial interval of Co

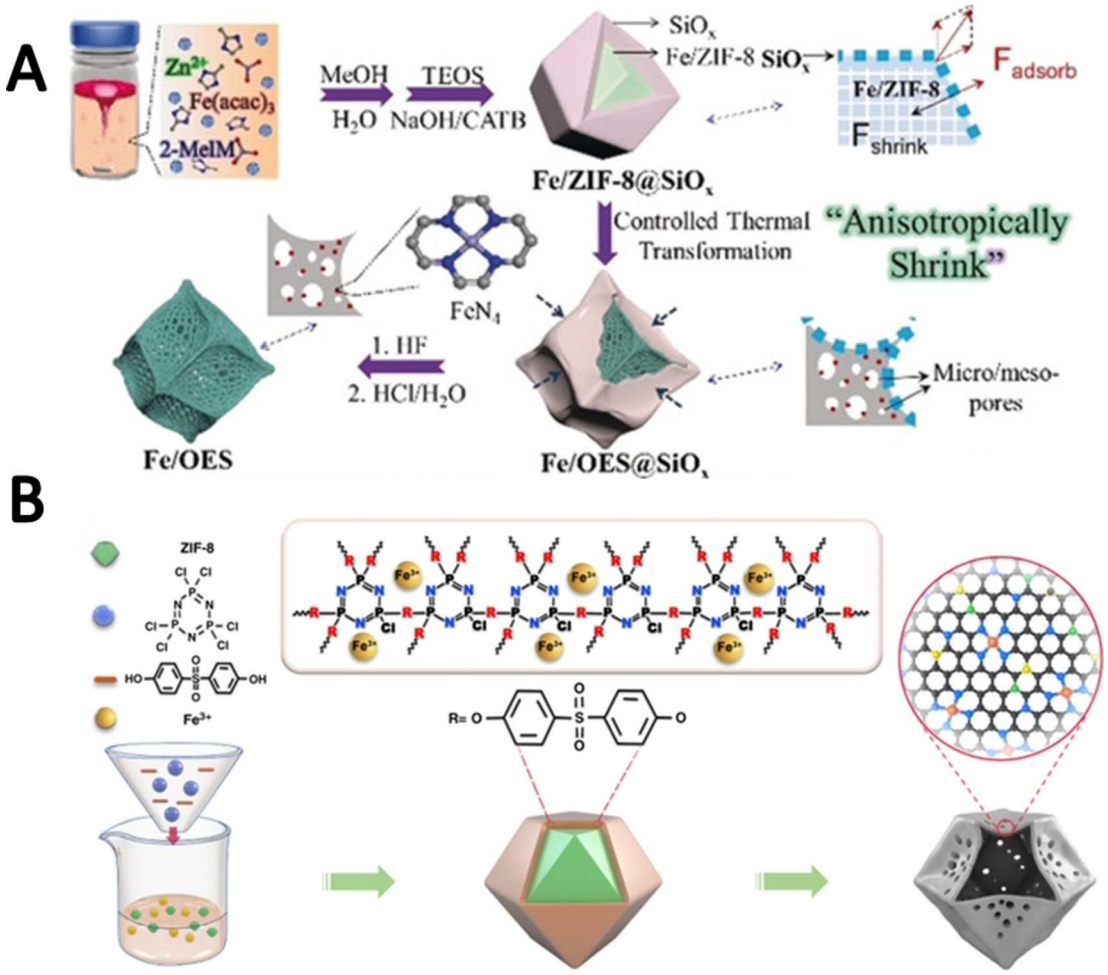

Figure 3. (A) Synthesis process of Fe/OES. Reproduced with permission.[70] Copyright 2020, Wiley-VCH. (B) Synthesis process of Fe-SAs/NPS-HC. Reproduced with permission.[71] Copyright 2018, Nature Publishing Group.

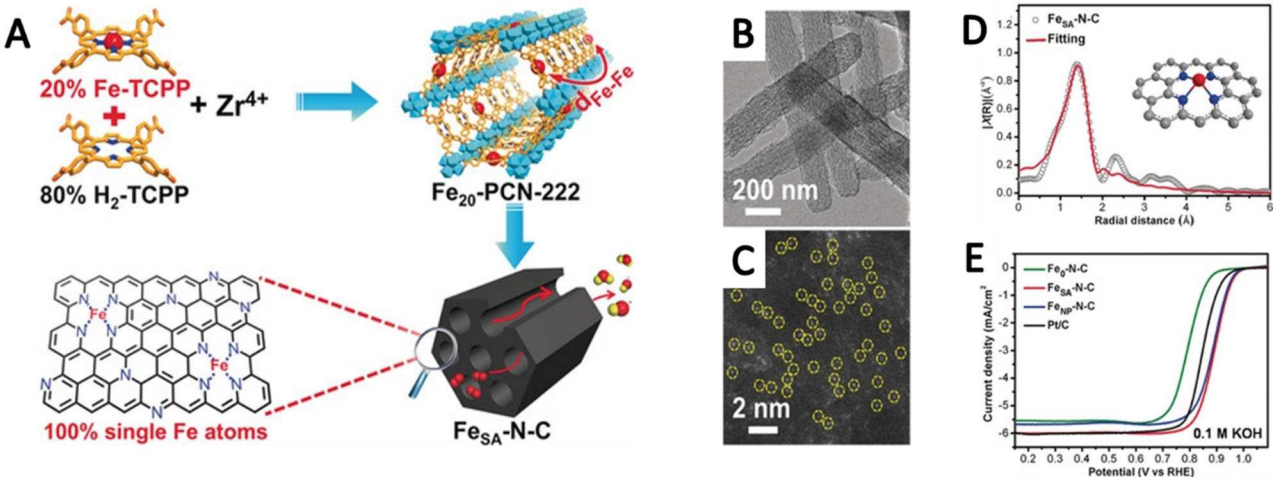

Figure 4. (A) Illustration for the synthesis of FeSA–N-C. (B,C) TEM and HAADF-STEM images of Fe_{SA}-N–C. (D) EXAFS fitting for Fe_{SA}-N–C. (E) LSV curves of various catalysts. Reproduced with permission.[72] Copyright 2018, Wiley-VCH.

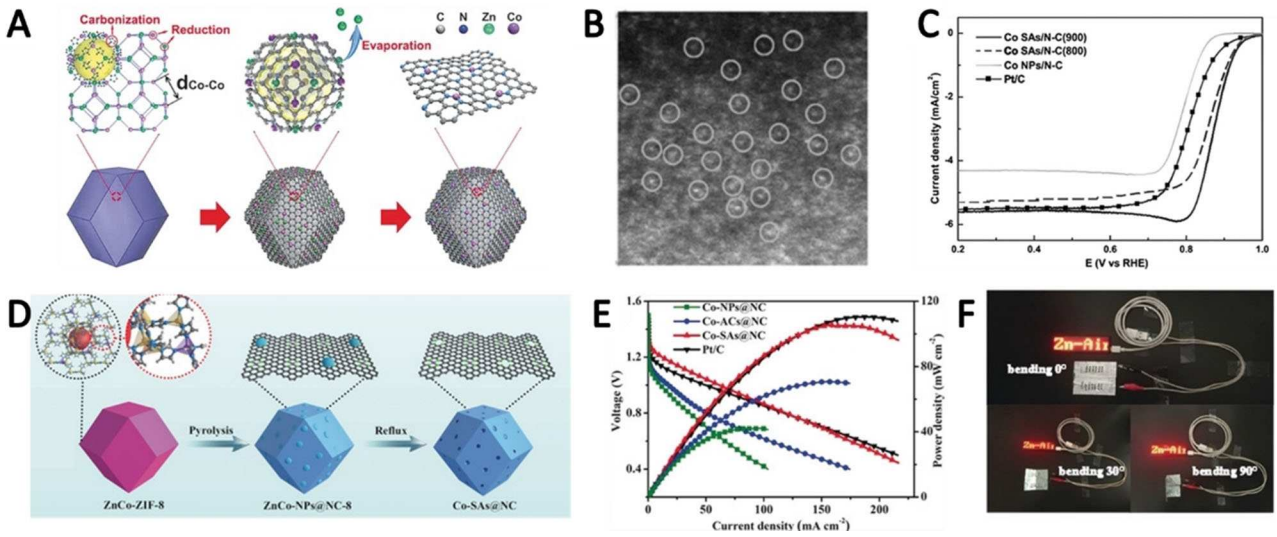

Figure 5. (A) Formation and Co SAs/N–C. (B) HAADF-STEM images of Co SAs/N–C. (C) LSV curves of various catalysts. Reproduced with permission.[50] Copyright 2016, Wiley-VCH. (D) Preparation of the Co-SAs@NC. (E) Polarization curves and power densities of the various catalysts. (F) Photographs of an LED screen powered by two Zn-air batteries with Co-SAs@NC catalyst. Reproduced with permission.[78] Copyright 2019, Wiley-VCH.

atoms but also generate free N sites to stabilize the Co atoms. When the Zn/Co ratio is above 1:1, Co single atoms in N doped carbon (Co SAs/NC) can be readily prepared at 800 or 900 °C. HAADF-STEM image clearly indicated the present of Co single atoms (Figure 5B) and EXAFS indicated that the Co is coordinated by N in the form of Co–N_4 and Co–N_2 in Co SAs/NC(800) and Co SAs/NC(900). The LSV curves clearly demonstrated the higher ORR catalytic activity of Co single atoms compared with Co nanoparticles (Co NPs/N–C), demonstrating the advantage of the Co single atoms (Figure 5C). In addition, this work also suggested that the coordination environment of Co atoms was very important, as indicated by the higher ORR performance of Co SAs/NC(900) than Co SAs/NC(800).

The size effect of Co-based catalysts for ORR was further investigated by Deng and co-workers, where Co nanoparticles (Co–NPs@NC), atomic Co clusters (Co-ACs@NC) and Co single atoms (Co-SAs@NC) anchored on N doped carbon were prepared by controlling the Zn/Co ratio to 0:1, 2:1 and 8:1 in ZnCo-ZIF (Figure 5D).[78] When used for ORR catalysts, a trend of Co-SAs@NC > Co-ACs@NC > Co–NPs@NC were observed in terms of onset potentials, half-wave potentials and kinetic current densities. In addition, Co-SAs@NC based Zn-air battery also exhibited higher power density than the other two catalysts, comparable with that for commercial Pt/C catalyst (Figure 5E). Moreover, two connected flexible batteries in series could effectively power a light-emitting diode screen, demonstrating the practical applications of the Co-SAs@NC (Figure 5F).

Generally, the structure model for Co–N–C catalysts are usually a Co atom connected by several N atoms (typically 4) in an intact graphitic layer (Co–N_4 moiety).[79–81] In a recent work, Wu and co-workers reported a Co SAC (Co–N–C) with CoN_{2+2} sites (Co–N_4 moiety bridging two neighboring armchair graphitic edge) using a surfactant-assisted MOF thermal annealing strategy, as shown in Figure 6A.[82] The cohesive interface interaction of Co-doped ZIF-8 and the surfactant could avoid the collapse of the internal carbon framework through confinement effect, and prohibited the aggregation of adjacent Co single atoms. Therefore, the Co–N–C@ surfactant catalysts exhibited higher density of CoN_4 active sites than surfactant-free catalyst. In addition, the DFT calculation based on CoN_4 and CoN_{2+2} moieties showed that the CoN_{2+2} moiety had lower activation energy for the dissociation of OOH (a rate-determining step for ORR), demonstrating the importance role of coordination environment (Figure 6B).

As can be seen from the above discussion, the metal atoms are mainly focused on Fe and Co atoms, while other metals atoms are rarely investigated. In addition, the large-scale preparation of SACs is also a challenge.[83] In 2018, Li and coworkers developed a strategy to synthesize SACs using bulk metal as metal sources on a large-scale.[84] As exhibited in Figure 7A, NH_3 was used to drag Cu atoms from Cu foam during the pyrolyzing process of ZIF-8. The formed volatile $Cu(NH_3)_x$ species can be trapped by the defects of the N-doped carbon to facilitate the formation of single Cu atoms. The Cu atoms are coordinated by four N atoms to form CuN_4 moiety, which could stabilize the Cu atoms. In addition, the catalyst could be prepared in gram grade yield and the ZIF-8 can be instead by graphene and Cu atoms can be replaced by Ni or Co, demonstrating the large-scale synthesis and universality of this strategy. The LSV curves indicated that the catalytic activity toward ORR of Cu-SAs/NC is much better than pyrolyzed ZIF-8 and even surpassing commercial Pt/C catalyst (Figure 7B).

Since Fe based catalysts could participate and/or promote the Fenton reactions ($Fe^{2+} + H_2O_2$), which can cause the dissolve of Fe species, as H_2O_2 is a byproduct of the two-electron ORR. However, Fenton reactions involving Mn ions are insignificant owing to the weak reactivity between Mn and H_2O_2. Based on this consideration, Wu and co-workers developed single MnN_4

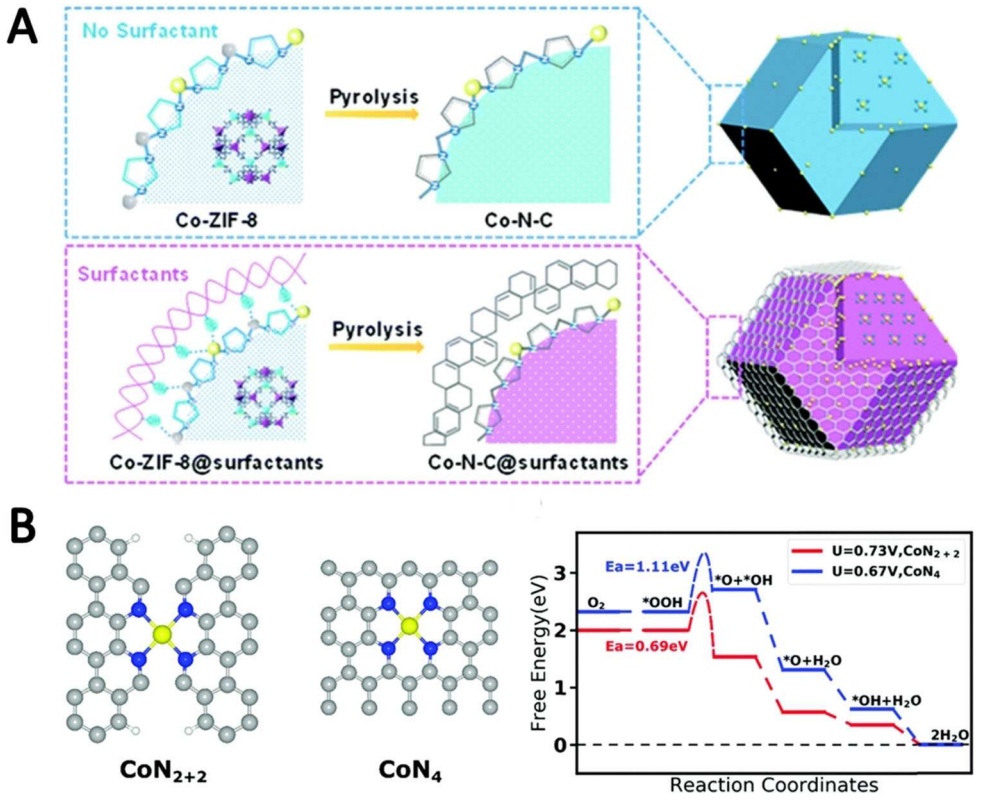

Figure 6. (A) Proposed strategy for the synthesis of Co–N–C@surfactants catalysts with increased active site density. (B) Structure of CoN_{2+2} and CoN_4 sites and free energy evolution diagram for $4e^-$ ORR pathway on the CoN_{2+2} site under a limiting electrode potential of U = 0.73 V and on CoN_4 site under a limiting electrode potential of U = 0.67 V. Reproduced with permission.[82] Copyright 2016, Royal Society of Chemistry.

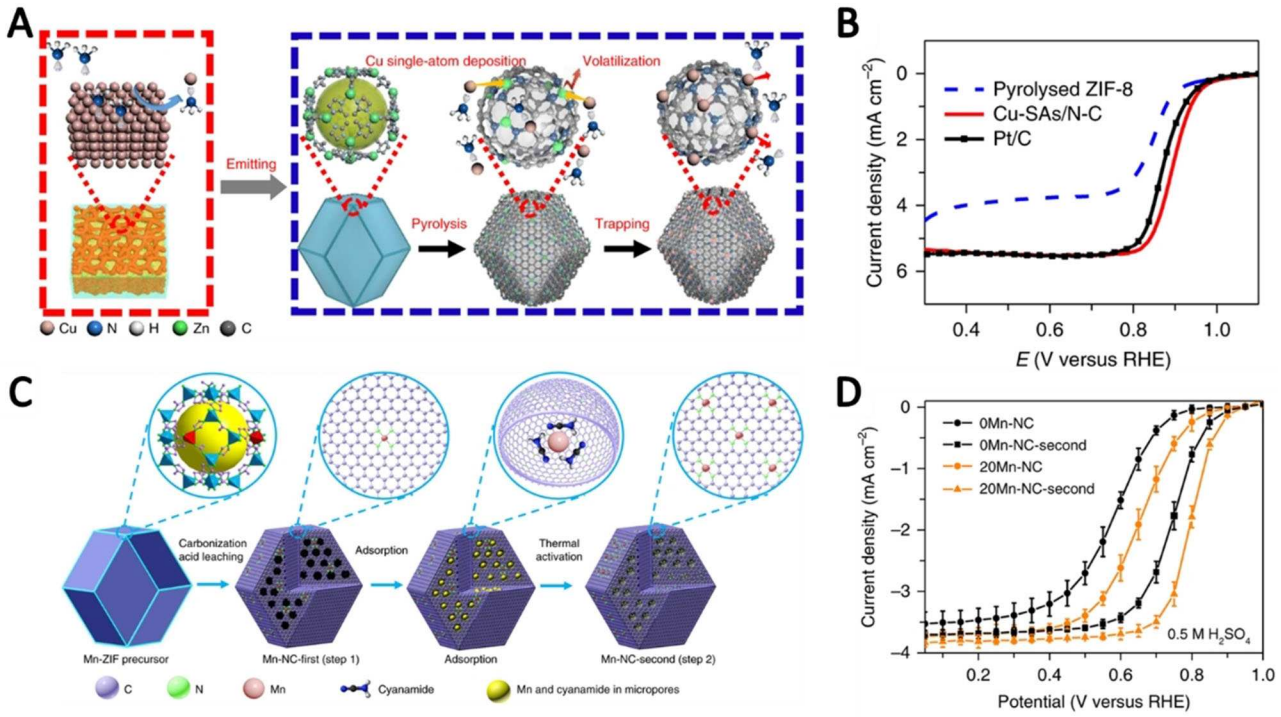

Figure 7. (A) Proposed reaction mechanism for the synthesis of Cu-SAs/N–C. (B) LSV curves of the various catalysts. Reproduced with permission.[84] Copyright 2018, Nature Publishing Group. (C) Schematic illustration for the synthesis of MnN_4 site catalyst. (D) LSV curves of the various catalysts. Reproduced with permission.[85] Copyright 2018, Nature Publishing Group.

moiety imbedded in N-doped carbon for fuel cells by a two-step method using Mn-doped ZIF-8 as a precursor (Figure 7C).[85] Since Mn ions are hard to exchange the original Zn in the ZIF-8, 20% Zn was replaced by Mn was chosen for detailed investigated. However, after pyrolyzing, the Mn content was only 0.68 wt% in 20Mn-NC. Thus, $MnCl_2$ and cyanamide was adsorbed in 20Mn-NC to prepare 20Mn-NC-second via further thermal activation. As a result, the Mn content increased to 3.03 wt% and is still in the form of single atoms. Compared with the catalysts without Mn and 20Mn-NC, 20Mn-NC-second exhibited much higher ORR catalytic activity in terms of onset potentials and half-wave potentials (Figure 7D).

As shown above, most of the SACs for ORR are based on Fe and Co atoms, and both Fe and Co could participate the Fenton reactions, which is a negative factor on the stability and activity of the SACs. Therefore, it is urgent to develop SACs based on other transitional metal atoms such as Mn, Cu, Zn or Ti to expand the types of SACs and obtain SACs with higher activity and stability.

2.2. SACs derived from MOFs for OER

OER plays a vital role in many electrochemical conversion devices such as water electrolyzer and rechargeable metal–air batteries.[86,87] In the OER process, the generated oxygen comes from the oxidation of hydroxyl or water molecules in the alkaline solution under acidic conditions and a series of oxygen adsorbates will generate, including HO*, O* and HOO*. This is a consequence of the transfer of electrons and protons, and the bonding interactions between these intermediates are crucial for catalytic activity. Too weak oxygen binding makes oxidation of HO* as a rate-determining step, while too strong oxygen binding makes the formation of HOO* as a rate-limiting step.[88,89] Therefore, it is of great significance to control the strength of oxygen bonding to promote the OER catalytic process.

Theoretically, the MOFs themselves can act as SACs owing to the single-atomically dispersed metal ions in them. However, the low conductivity of MOFs restricts their applications in electrocatalysts. In addition, the metal ions in MOFs are usually fully coordinated by ligands and the accessible electrocatalysis active sites is few. Therefore, creating uncoordinated metal sites is important for electrocatalysis. In a recent work, using N_2 dielectric barrier discharge (DBD) plasma to treat ZIF-67, Wang and co-workers successfully removed some organic ligands from Co and introduced coordinately unsaturated metal sites in ZIF-67 (CUMS-ZIF-67; Figure 8A).[90] The HAADF-STEM images indicated that Co-species are dispersed in CUMS-ZIF-67 in the forms of single atoms (Figure 8B). LSV showed that the OER activity of CUMS-ZIF-67 improved greatly compared with pristine ZIF-67, demonstrating the important role of CUMS (Figure 8C). The DFT calculations also indicated that the knocking off one ligand from ZIF-67 can effectively reduce the overpotential for OER. Similarly, the same group also treated ZIF-67 with O_2 plasma. The O_2 plasma could effectively oxide some of Co^{2+} in ZIF-67 to CoO_x, which is very active for OER (Figure 8D).[91] In addition, the O_2 plasma treatment also created some macro and mesopore in the CoO_x-ZIF-67, which could greatly promote electrolye diffusion to the CoO_x active sites. The HAADF-STEM images showed that the CoO_x species is 0.2–0.3 nm, suggesting that the Co is dispersed in atomic-scale (Figure 8E). The OER measurements showed that the OER

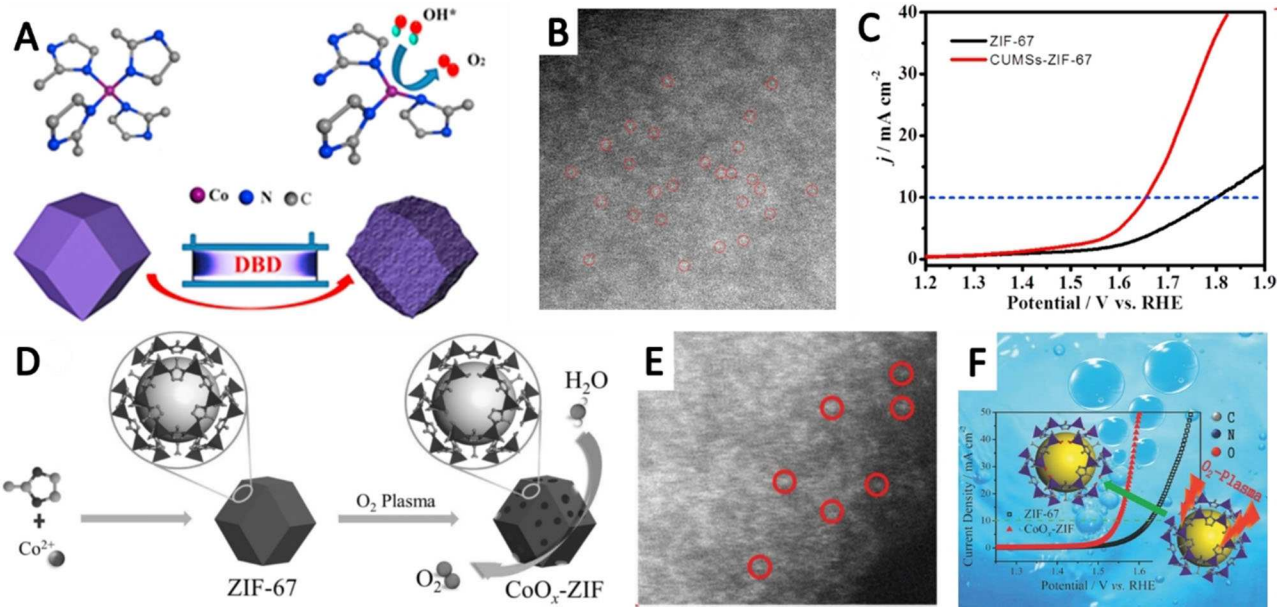

Figure 8. (A) Illustration for the synthesis of CUMSs-ZIF-67. (B) HAADF-STEM image of CUMSs-ZIF-67. (C) LSV curves of ZIF-67 and CUMSs-ZIF-67. Reproduced with permission.[90] Copyright 2017, Elsevier. (D) Preparation of CoO_x-ZIF. (E) HAADF-STEM images of CoO_x-ZIF. (F) Polarization curves of NC–Co SA and ZIF-67. Reproduced with permission.[91] Copyright 2017, Wiley-VCH.

activity of CoO_x–ZIF-67 was obviously higher than that of ZIF-67. Indeed, the CoO_x–ZIF-67 only needed a low overpotential of 318 mV at 10 mA cm^{-2}, which is much higher than that of ZIF-67 and comparable to commercial RuO_2 (Figure 8F). Moreover, the OER performance of CoO_x–ZIF-67 could be further improved by introducing carbon to enhance the conductivity of ZIF-67. This work indicated that not only single metal atoms can be prepared from MOFs, metal oxides active sites can also be obtained using MOFs as precursors.

The Co atoms not only exhibit high OER activity in the forms of CoO_x, but also in the form of N–Co bonding. Using Co–MOF nanoflake arrays on carbon cloth as precursor, Wang and co-workers prepared single atom Co catalysts imbedded in N-doped carbon (NC–Co SA) by carbonization and sequence acid leaching to remove extra Co clusters (Figure 9A).[92] The acid leaching not only lead to the formation of SACs, but also increased the porosity of the NC–Co SA. Compared with the NC–Co catalyst without acid leaching, the OER activity of NC–Co SA increased greatly, with overpotential of 360 mV to deliver a current density of 10 mA cm^{-2} (Figure 9B). In addition, the ORR catalytic activity of NC–Co SA is also better than that of NC–Co, with a high half wave potential of 0.87 V. Both the high OER and ORR activity of NC–Co SA enabled its high catalytic performance for a flexible Zn-air battery, with a high open-circuit potential of 1.41 V (this value for Pt/C is 1.27 V) and a low charging-discharging voltage gap of 0.45 V in flat states and 0.51 V in bent states (the values for NC–Co is 1.14 V in flat states and 0.52 V in bent states; Figure 9C), demonstrating the advantages of NC–Co SA for Zn-air batteries.

Though SACs have been utilized for OER, however, it should be noted that the OER performance of SACs is still lower than other advanced OER catalysts such as metal (hydro)oxides, and could not meet the demands of commercialization. The main reasons may be the low loading amount and limited coordination environment of the metals. For example, the metal loading in the SACs are usually less than 1.5 wt%, which greatly limited the density of metal active centers for OER. In addition, most of the SACs are based on M–N–C structure. However, it should be noted that metal sulfides and metal phosphides possess higher catalytic activity toward OER and HER based on the current research results. Therefore, it may be a good idea to design SACs based on M–S–C or M–P–C structure to improve the OER and HER performance of the SACs.

2.3. SACs derived from MOFs for HER

HER process can produce high purity hydrogen, which is a new clean energy alternative with carbon-free nature. However, the electrochemical production of H_2 is still not in industrial practice, mainly owing to the usage of precious metal catalysts to facilitate the HER kinetics.[93–96] Recent progress has demonstrated the great potential of transition metal based-SACs for HER both experimentally and theoretically.

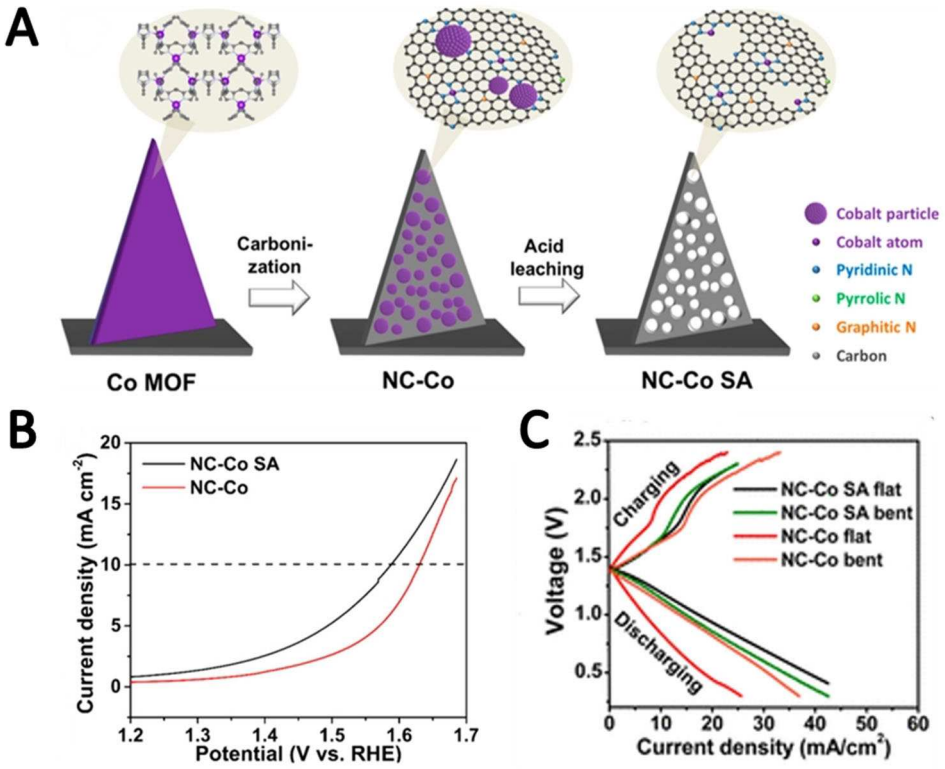

Figure 9. (A) Illustration of the preparation of NC–Co SA on carbon cloth. (B) LSV curves of NC–Co SA and NC–Co. (C) Polarization curves of NC–Co SA and NC–Co at flat and bent conditions. Reproduced with permission.[92] Copyright 2018, American Chemistry Society.

The SACs for HER was first investigated by Yao et. al in 2016, where a Ni-MOF was used as precursors to prepare Ni@C catalysts.[49] After further HCl leaching and an activation process by electrochemical cyclic-potential, single Ni atom catalysts anchored on carbon was obtained. The HCl leaching process removed most of the Ni clusters and Ni nanoparticles encapsulated with graphene layers are obtained (HCl–Ni@C). The thickness of the graphene layer is uneven and the acidic electrolyte (0.5 M H_2SO_4) could dissolve the Ni nanoparticles during the activation process, therefore atomically isolated Ni atoms are formed on the carbon (A–Ni–C). The LSV curves clearly indicated the huge activation trend of the catalysts, form overpotential of 440 mV for HCl–Ni@C to 34 mV for A–Ni–C, suggesting the superiority of single Ni atom catalysts.

The important role of single atoms for electrocatalysis were further demonstrated by Chen and co-workers, where ZnCo–biMOF and S–ZnCo–biMOF (ZnCo–biMOF with DMSO guest molecular) were pyrolyzed and further etched by acid.[97] The pyrolysis of ZnCo–biMOF resulted the formation of both Co nanoparticles and single atomic Co sites (Py-ZIF), while the pyrolysis of S–ZnCo–biMOF only leaded to the formation of single atomic Co (Co–SAC; Figure 10A). It is suggested that the S species could interacted with Co to form CoS_x species, which are readily dissolve in acid, and pure single atomic Co catalysts are obtained. The electrocatalytic measurement show that the Py-ZIF and Co–SAC exhibited almost the same catalytic activity toward HER and ORR (Figure 10B and 10C), indicating that the catalytic contribution mainly come from the atomic Co sites, once again demonstrating the advantages of single atom catalysts.

Tungsten-based materials such as WC, WN and WS_2 are also high active HER species.[98–100] In a recent work, single W atoms catalysts anchored on N doped carbon (W-SAC) were demonstrated to be more active than WC and WN.[101] As shown in Figure 11A, WCl_5 was first encapsulated in the framework of UiO-66-NH_2. The amine groups in UiO-66-NH_2 could effectively prohibit the W species from aggregation. After pyrolyzing the WCl_5/UiO-66-NH_2 composite and further etching the ZrO_2 by HF, W-SAC was prepared. The HAADT-STEM indicated that the W species were atomic dispersed in the catalysts and X-ray absorption fine structure (XAFS) spectroscopy suggested that the W atoms presented in the form of $W_1N_1C_3$ moiety (Figure 11B). The LSV measurements demonstrated the high catalytic activity of W-SAC, where only a low overpotential of

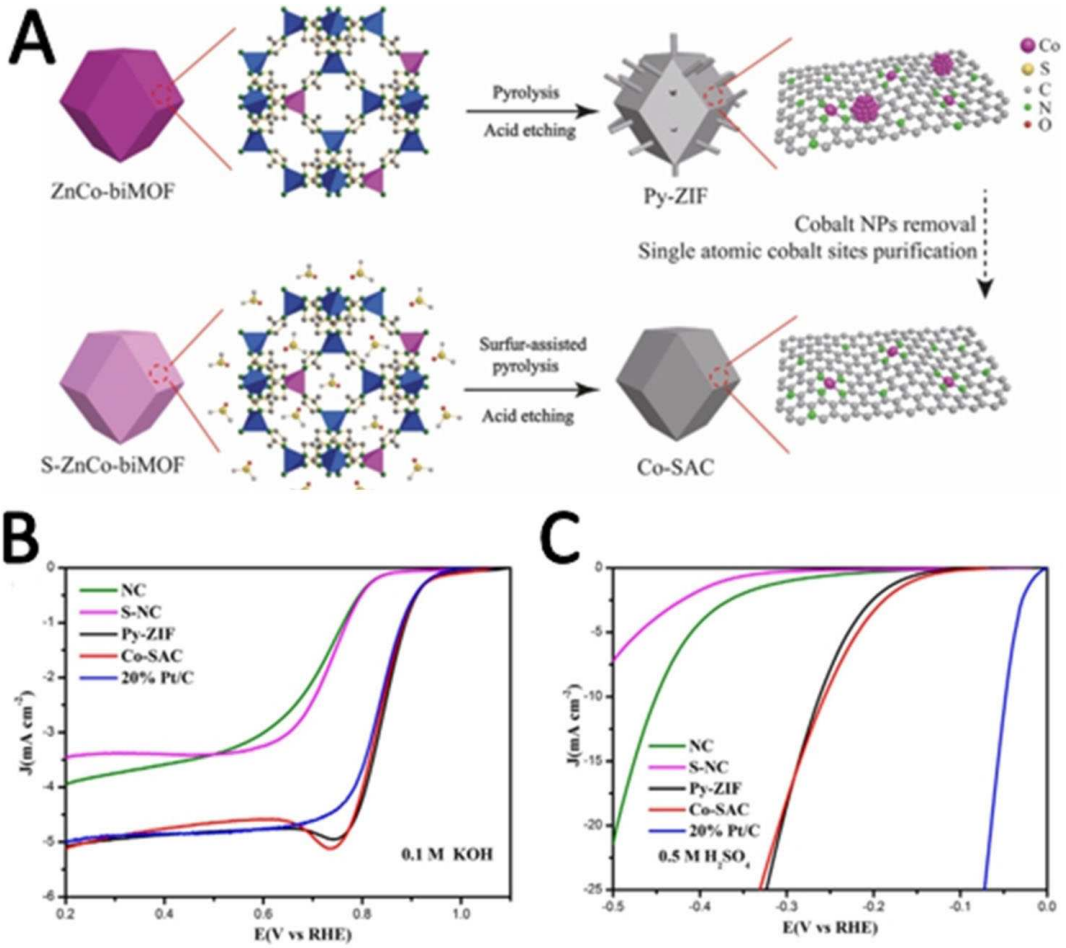

Figure 10. (A) Illustration of the coupled evolution of single-atom cobalt sites and metallic cobalt sites and their decoupling process. (B) LSV curves of the catalysts for ORR. (C) LSV curves of the catalysts for HER. Reproduced with permission.[97] Copyright 2018, Wiley-VCH.

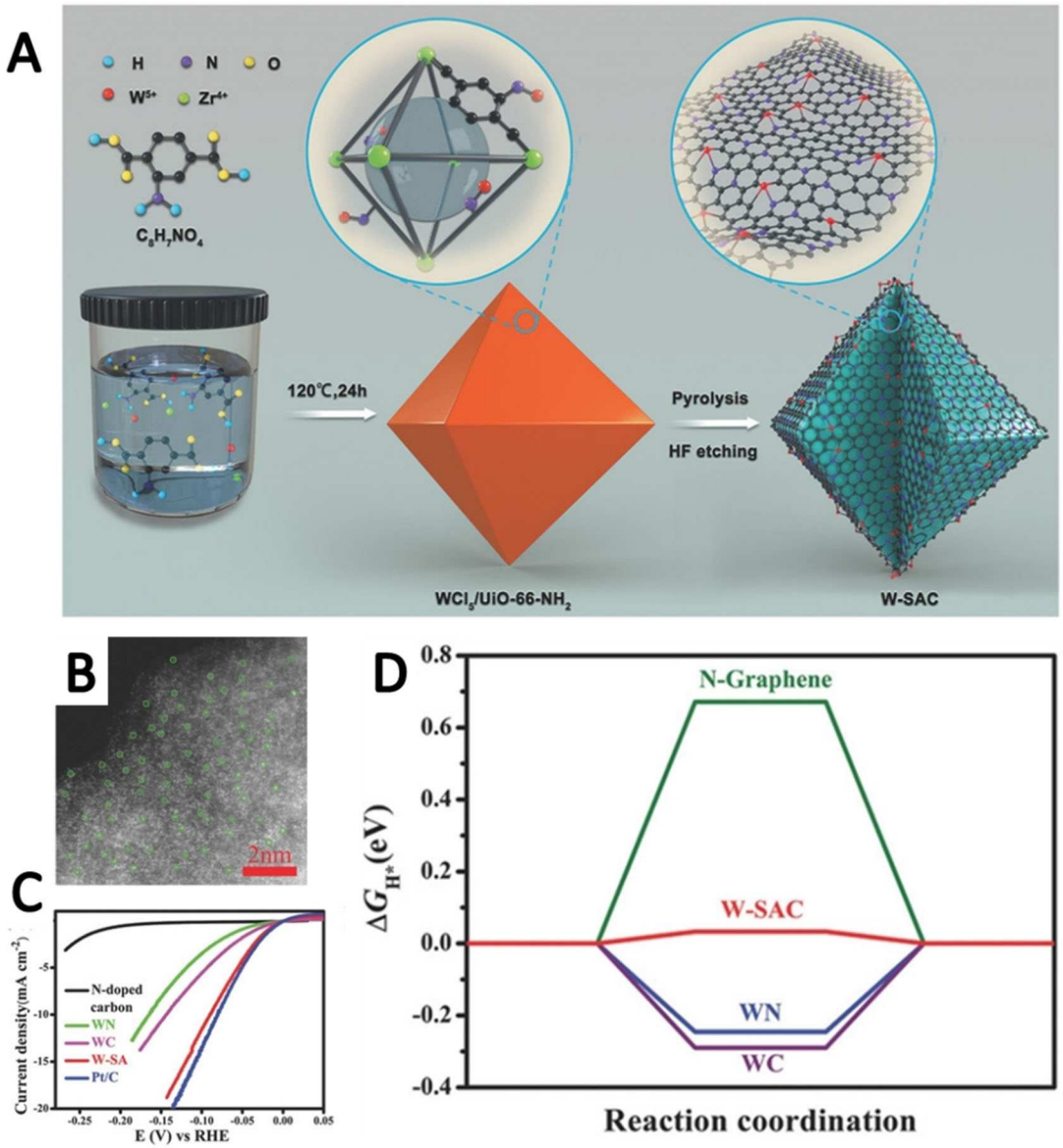

Figure 11. (A) Illustration for the preparation of W-SAC. (B) HAADF-STEM image of W-SAC. (C) HER performance of the various catalysts in 0.1 M KOH. (D) Gibbs free energy of hydrogen adsorption on the various catalysts. Reproduced with permission.[101] Copyright 2018, Wiley-VCH.

85 mV was needed at 10 mA cm^{-2} in 0.1 M KOH, much lower than that for WC (146 mV) and WN (169 mV; Figure 11C). The HER performance of W-SAC was also better than WC and WN in 0.5 M H_2SO_4. In addition, the ΔG_{H^*} for W-SAC was also smaller than that for WC and WN, indicating the high intrinsic catalytic activity of W-SAC (Figure 11D).

2.4. SACs derived from MOFs for CO_2 reduction

CO_2RR is an effective strategy to decrease the concentration of CO_2 in atmosphere using electricity generated by renewable energy sources such as wind and solar.[102] In addition, the CO_2RR can produce chemicals and fuels to realize the concept of carbon cycling. However, CO_2 is a very inert chemical owing to the high energy C=O bonds (806 kJ mol^{-1}). Meanwhile, the electrochemical CO_2RR is companied by HER, which can decrease the Faradaic Efficiency of CO_2RR.[103] Therefore, electrocatalysts that can active C=O as well as prohibited HER catalytic activity is very attractive for CO_2RR.[104]

Transition metal and their compounds especially M–N–C materials are promising candidates for CO_2RR owing to their appealing CO_2RR activity and selectivity. The coordination numbers of M–N–C catalysts have great effects on their activity toward CO_2RR. In a recent work, Wang et al. designed several Co SACs with different N coordination numbers by using mixed-metal ZIF (ZnCo-ZIF-67) as a precursor.[105] During the pyrolysis process, the Zn was evaporated away and Co ions were reduced by carbonized organic linkers to form atomically dispersed Co atoms embedded in N-doped carbon. By varying

the pyrolysis temperatures, Co single atoms imbedded in N doped carbon in the forms of Co–N_4, Co–N_3 and Co–N_2 were prepared at 800, 900 and 1000 °C respectively. HAADF-STEM images indicated the atomic dispersed Co atoms and EXAFS demonstrated the N coordination numbers. The CO_2RR measurements were carried in 0.5 M $KHCO_3$ solution and the results showed that the Co–N_2 catalyst had the best catalytic activity, with a high Faradaic efficiency of 95% at −0.68 V. The DFT calculations indicated that the Co–N–C catalysts with a low coordination number could promote the activation of CO_2 to CO_2^- intermediate.

The important role of coordination number of metal atoms in M–N–C catalysts was also demonstrated by Jiang and co-workers, where bimetallic MgNi-MOF-74 and polypyrrole (PPy) composite was chosen as a precursor (Figure 12A and 12B).[106] The Mg in the MOF can extend the spatial separation of Ni atoms and N atoms of PPy could anchor and stabilize Ni atoms to prohibit the formation of Ni clusters and NiO nanoparticles during the pyrolyzing process. By varying the calcination temperatures and removing MgO, Ni_{SA}–N_4–C, Ni_{SA}–N_3–C and Ni_{SA}–N_2–C could be readily prepared at 600, 800 and 900 °C. The three catalysts had similar Ni content (0.9 wt%) but different catalytic for CO_2RR, indicating the different catalytic activity induced by different N coordination number. The catalysts exhibited a trend of Ni_{SA}–N_2–C > Ni_{SA}–N_3–C > Ni_{SA}–N_4–C in activity, as indicated by the current density and Faradaic efficiency for CO. DFT calculation suggested that the reduction of CO_2 to CO is a two-proton and two-electron process and the formation of COOH* is the rate-determining step (Figure 12C and 12D). Ni_{SA}–N_2–C exhibited much lower ΔG for rate determination step than Ni_{SA}–N_4–C and Ni_{SA}–N_3–C, explaining its higher CO_2RR efficiency.

Except for the coordination number of metal atoms, the structural configurations also affect the CO_2RR performance of M–C–N catalysts. Using Fe or Co-doped ZIF-8 as precursor followed by thermal annealing, Li and co-workers prepared Fe and Co single atoms dispersed in N doped carbon (Figure 13A).[107] The catalytic measurements demonstrated the intrinsically higher catalytic of Fe–N_4 than Co–N_4. In addition, two kinds of structural configurations for Fe–N_4 was detected in the Fe–N–C catalyst. One is the Fe–N_4–C_{10} moieties imbedded in a graphitic layer and are fully encapsulated by C atoms. The other is the Fe–N_{2+2}–C_8 moieties, which composed by two armchair-like graphitic layers connected by Fe atoms and could cause a distortion of two adjacent carbon plane (Figure 13B). The latter structural configuration is more active than the form one based on the DFT results, providing guidelines for further designing of M–N–C catalysts for CO_2RR.

Bi-based materials are also promising catalysts to convert CO_2 into formate and CO.[108] To further improve the catalytic of Bi element, a Bi-based MOF and dicyandiamide (DCD) were used as precursors to prepare Bi SACs supported by N doped

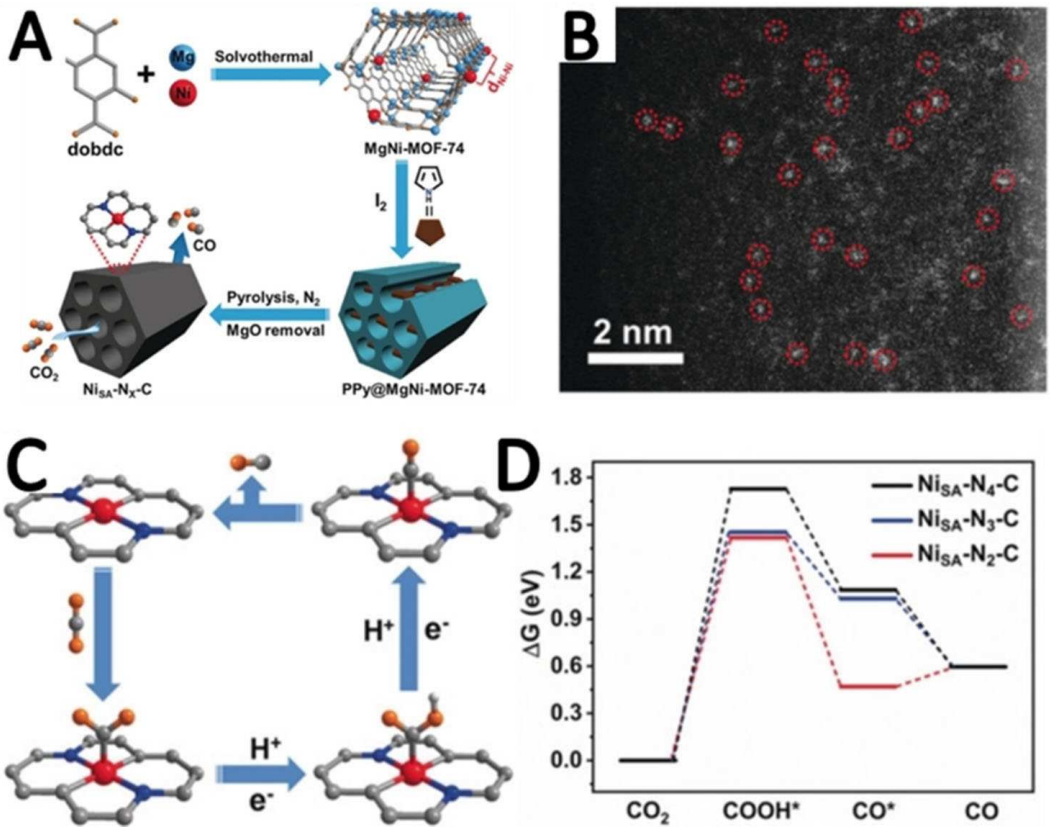

Figure 12. (A) Illustration for the preparation of Ni_{SA}-N_x-C. (B) HAADF-STEM image of Ni_{SA}-N_x-C. (C) Proposed reaction paths for CO_2RR using Ni_{SA}-N_2-C as a model. (D) Free-energy diagram of CO_2 reduction to CO over Ni_{SA}-N_x-C. Reproduced with permission.[106] Copyright 2020, Wiley-VCH.

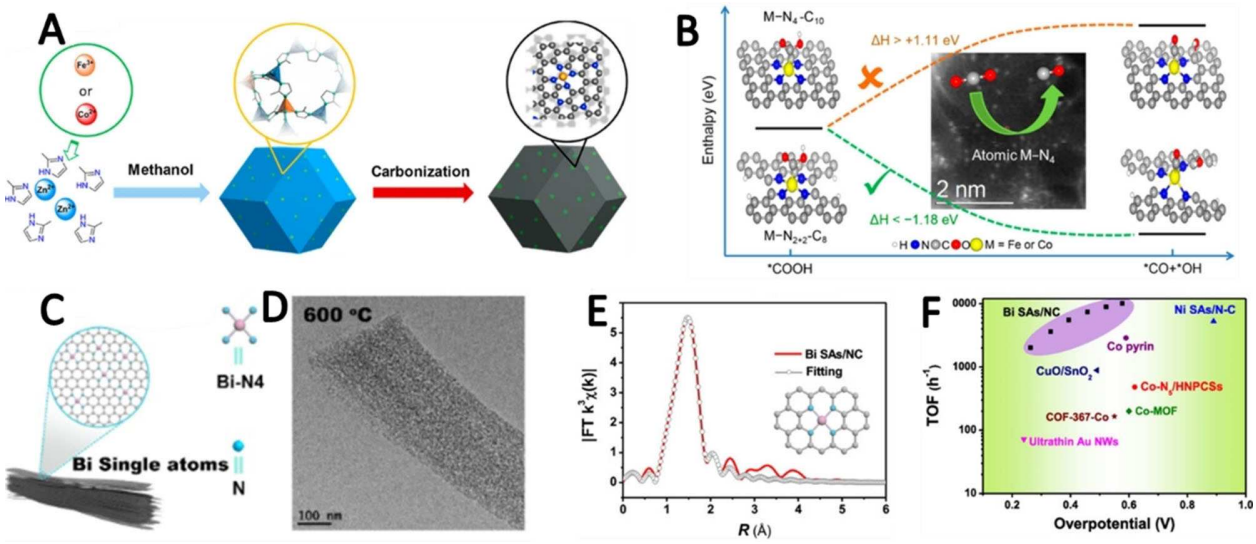

Figure 13. (A) Preparation of M–N-C catalysts. (B) Illustration for the effectiveness of CO_2RR on M-N_4-C_{10} and M-N_{2+2}-C_8 sites. Reproduced with permission.[107] Copyright 2018, American Chemistry Society. (C) Scheme for the Bi SAs/NC. (D) HAADF-STEM image of Bi SAs/NC. (E) EXAFS fitting for Bi SAs/NC. (F) TOF of the catalysts. Reproduced with permission.[109] Copyright 2019, American Chemistry Society.

carbon (Bi SAs/NC).[109] As shown in Figure 13C, the catalysts exhibited bundles-shaped morphology, similar with the pristine Bi-MOF. The calcination temperatures were crucial for the formation of the SACs as Bi nanoparticles were formed at 350–500 °C. When the temperature was increased to 600 °C, atomically dispersed Bi atoms were obtained and it is suggested the NH_3 released from the decomposition of DCD facilitated the atomization of Bi nanoparticles (Figure 13D). In addition, the DCD also introduced N atoms in the Bi SAs/NC and the Bi atom was coordinated by four N atoms to form the Bi-N_4 moieties (Figure 13E). The Bi SAs/NC exhibited much higher catalytic for CO_2RR, compared with Bi nanoparticles (Bi NPs/NC) and Bi clusters (Bi Cs/NC), as indicated by the LSV curves and Faradaic efficiency. Moreover, the Bi-N_4 moieties had a lower free energy for the formation of COOH* intermediate, suggesting its better performance.

For CO_2RR, owing to the different amounts of transferred electrons, it is possible to obtain different reduction products such as CO, HCOOH, CH_4, and C_2H_4 in the process of CO_2RR. However, the main product based on MOFs based SACs catalysts is CO, as demonstrated by the above examples. It should be noted that compared with CO, the products with high H/C ratio such as C_2H_4 and CH_4 are more desirable, and the related reported is rare. Therefore, it is still urgent to develop advanced catalysts that could converse CO_2 more effectively into CH_4, C_2H_4 and alcohols.[110]

2.5. SACs derived from MOFs for NRR

NH_3 is an important kinds of clean energy carrier as well as chemical for fertilizer synthesis and plays an indispensable role in the agricultural, pharmaceutical, plastic, and textile industries.[111] General, NH_3 is mainly produced based on Haber-Bosch process under high-temperatures (400–550 °C) and high-pressures (200–300 atm) using N_2 and H_2 as raw materials. This reaction takes up 1% total fossil energy and emits more than 450 million tons of carbon dioxide each year.[112,113] On the contrary, electrochemical NRR can produce NH_3 under ambient conditions and has attracted increasing investigation interests. Nowadays, the main challenge for electrochemical NRR is the development of NRR catalysts that can effectively adsorb and activate N_2. In addition, the Faradic Efficiency for NRR is seriously restricted by the competitive HER owing to the overlapped potential for NRR and HER and the faster HER kinetics.[114] Therefore, designing proper electrocatalysts that can weaken N≡N triple bond and suppress HER is very important.

Comparing with metal nanoparticles, the metal atoms with positive charge in SACs can restrict the adsorption of protons and only top site of SACs can be used for adsorbing proton. Therefore, the SACs may be good candidates to suppress HER and improve the faradaic efficiency of NRR. In a recent work, Jiang et. al. prepared single-atom Fe anchored on N-doped carbon (Fe_1–N–C) using a mix-ligand MOF as a precursor.[115] Using Fe-TCPP (iron(III) meso-tetra(4-carboxyphenyl) porphine chloride) and H_2-TCPP (tetra (4-carboxyphenyl) porphine) as mixed ligands, the distance of Fe atoms PCN-222 could be extended to promote the formation of Fe single atoms in the Fe_1-N–C (Figure 14A). The TEM and HAADF-STEM images clearly indicated the rod-like morphology of Fe_1–N–C and the presence of single Fe atoms (Figure 14B and 14 C). XANES suggested that the Fe probably present in the form of Fe_1-N–C in the catalysts. In addition, compared with Co_1–N–C and Ni_1-N–C prepared by similar strategy, the Fe_1-N–C exhibited higher NH_3 yield (1.56×10^{-11} mol cm^{-2} s^{-1}) and faradaic efficiency (4.51%). Furthermore, the DFT calculation indicated that the Gibbs free energy for the rate determination step (N_2* to N_2H*) of Fe_1–N–C is the smallest.

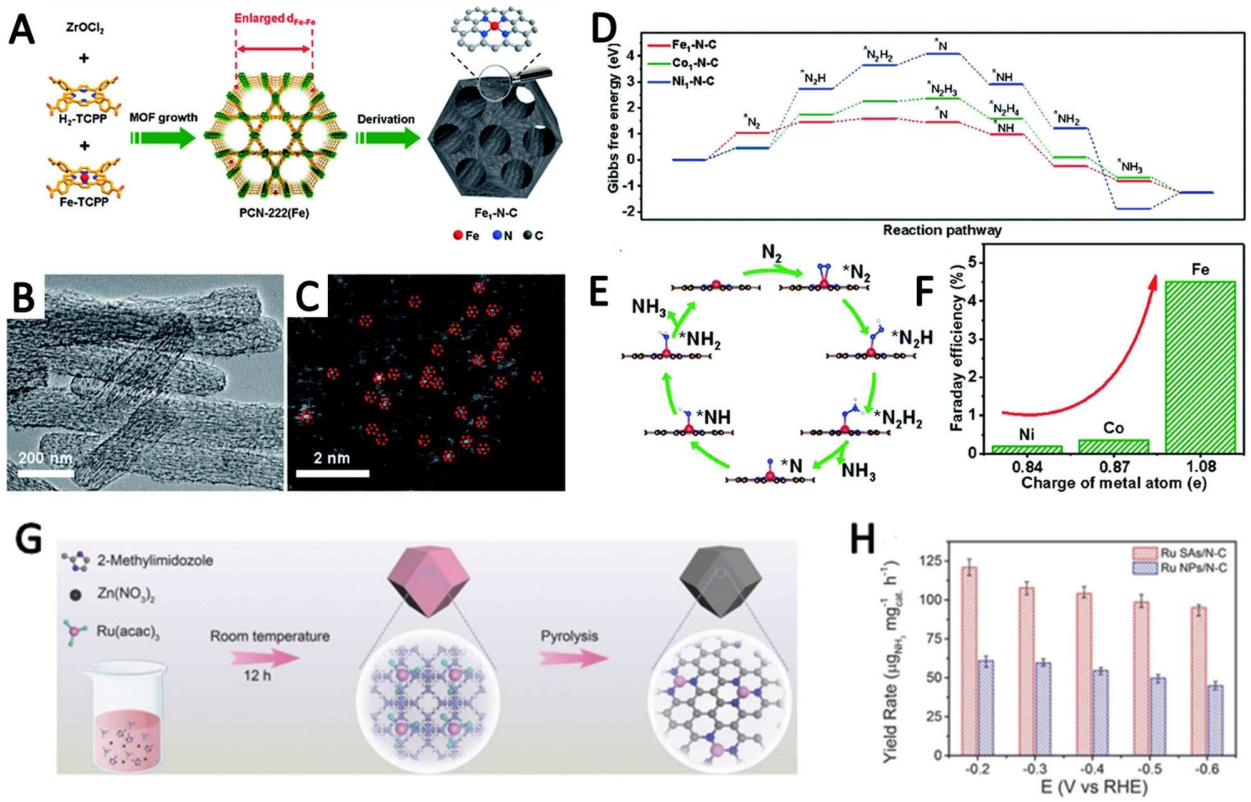

Figure 14. (A) The fabrication of Fe_1-N–C from PCN-222(Fe). (B,C) TEM and HAADF-STEM images of Fe_1-N–C. (D) Free energy plot, of the NRR on the M_1-N–C. (E) The intermediates in the distal path of the NRR on Fe_1-N–C. (F) The Bader charge analysis of M_1-N–C. Reproduced with permission.[115] Copyright 2019, Royal Society of Chemistry. (G) Scheme for the synthesis of Ru SAs/N–C. (H) Yield rate of NH_3 on Ru SAs/N–C and Ru NPs/N–C at various potentials. Reproduced with permission.[52] Copyright 2018, Wiley-VCH.

Bader charge analysis showed that Fe atom possess more positive charge, which could restrain the HER process effectively (Figure 14D-14F).

Metal Ru is also an efficient element that can adsorb N_2 and activate N≡N triple bond. Using Ru and Zn as metal centers to construct ZIF-8 followed by pyrolyzing, Ru single atoms dispersed in N doped carbon (Ru SAs/N–C) were prepared (Figure 14G).[52] EXAFS result showed that Ru atoms were coordinated by N atoms and no metallic Ru or Ru_xO_y were observed. Compared with the Ru nanoparticles on carbon (Ru NPs/N–C) prepared by increasing the Ru content in the ZIF-8 framework, the Ru loading in the Ru SAs/N–C is much lower (0.18 wt% vs. 2.64 wt%). However, the Ru SAs/N–C exhibited much higher NH_3 yield at the measured potentials. Especially, at −0.2 V, Ru SAs/N–C exhibited a high NH_3 yield of 120.9 $\mu g\, mg_{cat.}^{-1}\, h^{-1}$, demonstrating the high potentials of Ru SACs (Figure 14H). The DFT calculation indicated that N_2 dissociation is the rate-limiting step for Ru (101) and N-coordinated Ru single atoms (Ru_1–N_3), and the ΔG of N_2 dissociation on Ru_1–N_3 is smaller than that for Ru (101), indicating the high intrinsic activity of the Ru SAs/N–C.

As stated above, the structures of SACs are mainly M–N–C, where the N atoms are always involved in the carbon substrate. However, it should be noted that for NRR, the impurities of raw materials and less standard operation may produce false results. For example, it is point out that some of the detected NH_3 may come from the decomposition of catalysts or the surrounding environment, especially for metal nitrides and N-containing catalysts. Therefore, we should be more careful when determine the catalytic activity of SACs catalysts, and at least high-purity isotopes measurements should be conducted to determine the sources of product NH_3.[116,117]

3. Dual-atom Electrocatalysts Derived from MOFs

Compared with SACs, dual-atom catalysts (DACs) with more flexible active sites and higher metal loading are more attractive. In addition, the electronic structures of the DACs can be more readily adjusted by introducing heteronuclear metal atoms with different d-band configuration to regulate the adsorption energies of intermediates.[118–121]

Recently, Liao and co-workers reported single/paired Fe atoms on porous carbon nanosheet (Fe/N-PCNs) for ORR using a 2D Zn/Fe-MOF as a precursor with the assistance of g-C_3N_4 (Figure 15A).[122] The Zn^{2+} extend the distance of Fe atoms in the MOF and g-C_3N_4 also served as stabilizer to prohibit the aggregation of Fe atoms. The HAAD-STEM image indicated the

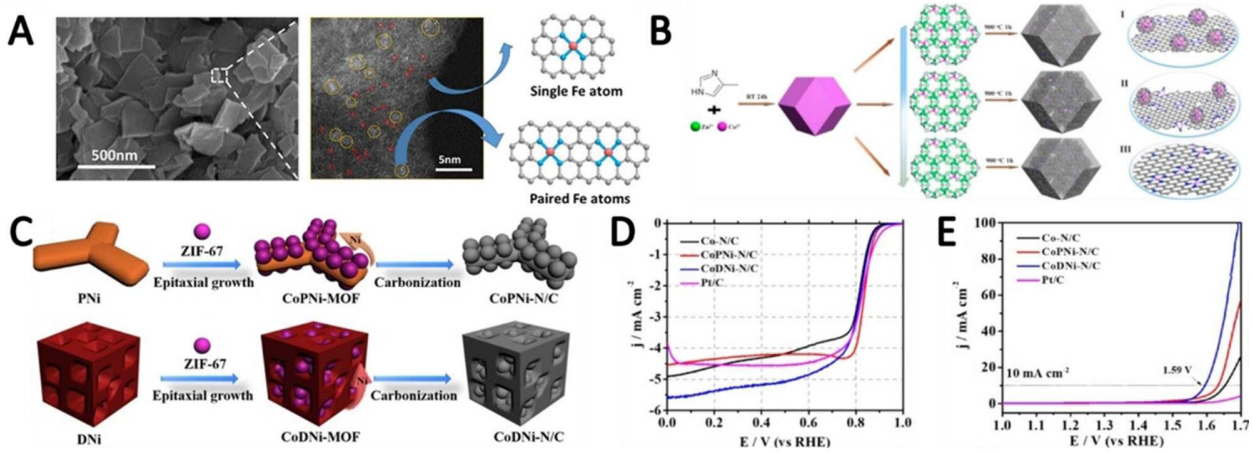

Figure 15. (A) SEM and HAADF-STEM images of the Fe/N-PCN catalyst. Reproduced with permission.[122] Copyright 2020, American Chemistry Society. (B) Illustration for the controllable preparation of the Co–N–C-x catalysts with varied active site structures. Reproduced with permission.[123] Copyright 2020, Elsevier. (C) Schematic illustration of the preparation of CoPNi–N/C and CoDNi–N/C. (D–E) ORR and OER activity of the catalysts. Reproduced with permission.[124] Copyright 2019, Elsevier.

existence of both single Fe atoms and paired Fe atoms and the loading of Fe was determined to be as high as 3.89 wt%. Owing to the high-density active sites, the Fe/N-PCNs exhibited better catalytic performance toward ORR than commercial Pt/C catalyst in terms of higher half-wave potential in 0.1 M KOH and better durability.

In another work, Xing and co-workers demonstrated that binuclear Co_2N_5 sites were more active than CoN_4 sites.[123] As shown in Figure 15B, by controlling the Zn/Co ratio to 5:1, 10:1 and 50:1, Co embedded in N doped carbon (Co–N–C-x, x means the ration of Zn/Co) in various forms are prepared. In detail, Co–N–C-50 only possessed CoN_4 sites in single-atom size and Co–N–C-5 had large Co nanoparticles and CoN_4 sites. In contrast, Co–N–C-10 had Co nanoparticles and binuclear Co_2N_5 active sites, as indicated by both HAADF-STEM image and EXAFS curve. The ORR performance of Co–N–C-10 was better than the other two catalysts and the DFT calculations revealed that the Co_2N_5 site exhibited reduced thermodynamic barrier for ORR, paving a new way for designing M–N_x–C catalysts.

Compared with homonuclear DACs with the same metal atoms, the heteronuclear DACs with different kind of metal sites are more attractive owing to the synergistic effect of different metal atoms. By epitaxial growth of ZIF-67 on tris-1,10-phenanthroline nickel(II) nitrate (PNi), CoPNi-MOF was prepared and used as a precursor to prepare Co/Ni atoms imbedded in N-doped carbon for electrocatalysts (Figure 15C).[124] Owing to the high metal contents in the MOF, NiCo alloy nanoparticles were formed in the obtained CoPNi–N/C. In addition, HAADF-STEM image also demonstrated atomic Co/Ni dual sites in the CoPNi–N/C. Moreover, this strategy could be well extended when the PNi was changed to dimethylglyoxime nickel(II; DNi; Figure 15C). The LSV measurement indicated that the catalytic performances of CoPNi–N/C and CoDNi–N/C are better than the Co–N/C derived form ZIF-67 (Figure 15D and 15E). DFT calculations suggested that the higher activity could be ascribed to the synergetic effect of Co/Ni-N–C bonds.

The synergistic effect of Co and Fe dual sites was demonstrated in a work reported by Li and co-workers, where $FeCl_3$ was encapsulated in the cavities of ZnCo-ZIF-8 (Figure 16A).[125] After pyrolyzing at high temperatures, the Fe^{3+} was reduced and the formed Fe species could catalyze the decomposition of the of metal-imidazolate-metal linkages to form large voids inside MOFs. The dual-sites of (Fe, Co)/N–C were demonstrated by the HAADF-STEM images and the (Fe,Co)/N–C adopted a porphyrin-like dual metal center (Figure 16B and 16 C). The ORR measurement demonstrated the better performance of (Fe, Co)/N–C compared with Fe SAs/N–C and Co SAs/N–C and DFT calculation indicated that (Fe, Co)/N–C could decrease the cleavage barrier of O–O bond to favor four electron ORR pathway. In another work, the advantage of Fe–Co dual sites for the activation of oxygen by weakening the O=O bond were also demonstrated.[126]

Besides ORR, the synergistic effect of DACs was also observed in CO_2RR. By using Fe-doped ZIF-8 to adsorb Ni^{2+}, a Zn/Ni/Fe ZIF was prepared and used as a precursor to prepare diatomic Ni–Fe sites supported by N-doped carbon (Ni/Fe–N–C; Figure 16D).[127] The current density for CO_2RR to generate CO for Ni/Fe–N–C at −0.7 V is 4.6 and 1.5 times higher than that for Fe–N–C and Ni-N–C. In addition, the much higher turnover frequency of Ni/Fe–N–C (7680 h^{-1}) compared with Fe–N–C (813 h^{-1}) and Ni-N–C (3690 h^{-1}) also demonstrated the high intrinsic activity of Ni/Fe–N–C. DFT calculation indicated that the Ni/Fe–N sites would change into a CO adsorbed moiety upon CO_2 uptake, which could reduce the energy barrier for the formation of COOH* intermediate and the desorption of CO, resulting in the good CO_2RR activity (Figure 16E).

4. Summary and Outlooks

Metal-organic frameworks (MOFs)-derived atomic electrocatalysts have demonstrated great potentials in various electro-

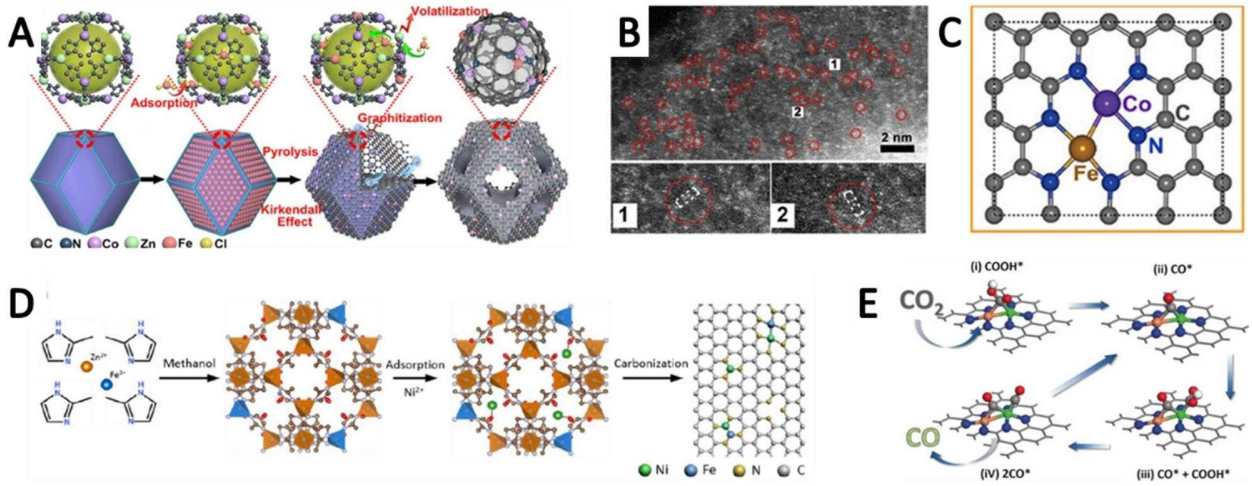

Figure 16. (A) Preparation of (Fe,Co)/N–C. (B) HAADF-STEM images of (Fe,Co)/N–C. (C) Proposed atomic structure of (Fe,Co)/N–C. Reproduced with permission.[125] Copyright 2017, American Chemistry Society. (D) Synthesis procedure of Ni/Fe–N–C. (E) The catalytic mechanism on diatomic metal-nitrogen site based on the optimized structures of adsorbed intermediates COOH* and CO*. Reproduced with permission.[127] Copyright 2019, Wiley-VCH.

catalysis reactions owing to their high catalytic activity and maximum utilization of active sites. In this Review, the research progress of single-atom catalysts (SACs) and dual-atom catalysts (DACs) derived from MOFs toward the oxygen reduction reaction (ORR), oxygen evolution reaction (OER), hydrogen evolution reaction (HER), CO_2 reduction reaction (CO_2RR) and nitrogen reduction reaction (NRR) are summarized. Especially, the synthesis strategies, chemical structures and catalytic performances of the catalysts are addressed to give researches a deep comprehension on the strategies to prepare atomic catalysts from MOFs and the means to improve the performance of the catalysts. Indeed, MOFs-based atomic catalysts are attracting ever-increasing attentions with the development of advanced synthesis and characterization methods.

Although MOFs-based atomic catalysts have achieved great progress in a very short timeframe. However, it should be mentioned that this kind of catalysts is still in the exploration stage and there are still great challenges for their further development in both synthesis and application aspects.

(i) At present, only several MOFs, such as ZIF-67, MIL-101 and ZIF-8, are extensively investigated as precursors for preparation of atomic catalysts and the metal sites are limited to Fe, Co, Ni. This not only limited the metal active sites, but also restrict the diversity of carbon supports for the similar ligands such as 2-methylimidazole, (2-amino) terephthalic acid in these MOFs. To extend the diversity of atomic electrocatalysts derived from MOFs, MOFs with different metal centers and ligands should be investigated, especially mixed metal MOFs to adjust the electronic structures of the catalysts via the synergistic effect of different active sites.

(ii) High-density active sites are indispensable to improve the catalytic activity on an electrocatalysts. For example, in a recent work, the metal loading of single-atomic-site (SAS) catalyst SAS–Fe achieves a record value of 30 wt% and the SAS–Fe show unprecedented catalytic performance for epoxidation of styrene using O_2 as the only oxidant (yield: 64%; selectivity:89%).[83] However, the metal loadings of mostly reported atomic catalysts are usually less than 1.5 wt%, which limited the further improvement of their catalytic activity. The synthesis of atomic catalysts with high metal loading is still very challenging. Designing proper supports with more cheating sites may be a promising method. From the viewpoint of MOFs, the metal contents in pristine MOFs are high enough and it is urgent to develop more mild synthesis method to avoid the aggregation of metal centers during the post fabricating process.

(iii) Nowadays, most of the MOFs derived atomic electrocatalysts are their ORR performance and lots of catalysts show superior ORR activity than commercial Pt/C catalysts. However, many energy conversion devices need bifunctional electrocatalysts to simplify the operating systems. For example, the metal–air batteries need bifunctional ORR and OER catalysts and water-splitting devices demand catalysts that are both active for HER and OER. Obviously, the OER and HER performance of most of the electrocatalysts are not satisfactory and could not comparable with many other electrocatalysts such as meta (hydro) oxides, metal sulfides and so on. The CO_2RR and NRR catalysts also face the issues of low activity and selectivity. The main reasons for this may be owing to the low-density active sites. Therefore, more efforts are needed to devote to the development of bifunctional catalysts by improving the OER and HER performance of atomic catalysts.

(iv) Developing DACs could effectively improve the density of active sites to some extent, and the synergistic effect of different metal atoms could further enhance the catalytic performance of DACs. However, the preparation of DACs with uniform and highly dispersed dual atoms is more challenging. On the one hand, the multiple metal atoms are more prone to aggregation or alloying owing to the

increase metal density in the precursors. On the other hand, the coordination abilities of organic ligands with various metal centers are different and it is difficult to precisely control the metal ratio in the pristine MOFs, which in turn make it difficult to control the metal ratio in DACs. This not only restrict the full utilization of synergistic effect between different metal atoms, but also bring difficulties in accurate identification of active sites in DACs. Therefore, it is urgent to develop more effective synthetic strategy for preparing DACs.

(v) The surface energy of single metal atoms is very high and they are readily to aggregation with each other to form metal nanoclusters or nanoparticles. Therefore, the stability of SACs should be improved by strength the interactions of metal atoms with the surrounding substrates. In addition, most of the literatures only reported the catalysts' state before the catalytic reaction and the forms of metal atoms after long-term cycling is rarely reported. This not only limited the understanding of stability, but also restrict the inference of catalytic mechanism. Therefore, to give researches deep understanding of the stability and catalytic mechanism of SACs, operando or post characterization technologies should be utilized to monitor the reaction processes and reveal reaction mechanisms.

Overall, the development of atomic catalysts form MOFs is exciting and challenging. However, it is no doubt that the atomic catalysts will still undergo rapid development and more efficient atomic electrocatalysts can be expected based on the continuous research efforts.

Acknowledgements

This work has been financially supported by the National Natural Science Foundation of China (No. 21902189 and 21901264), Key Scientific Research Projects of Universities in Henan Province (21A150062) and Young Backbone Teacher of Zhongyuan University of Technology.

Conflict of Interest

The authors declare no conflict of interest.

Keywords: Electrocatalysis · dual-atom catalysts · metal-organic frameworks · MOF derivatives · single-atom catalysts

[1] L. Yang, J. Shui, L. Du, Y. Shao, J. Liu, L. Dai, Z. Hu, *Adv. Mater.* **2019**, *31*, 1804799.
[2] C. Hu, L. Zhang, J. Gong, *Energy Environ. Sci.* **2019**, *12*, 2620–2645.
[3] Y. Zhang, L. Tao, C. Xie, D. Wang, Y. Zou, R. Chen, Y. Wang, C. Jia, S. Wang, *Adv. Mater.* **2020**, *32*, 1905923.
[4] H. F. Wang, L. Chen, H. Pang, S. Kaskel, Q. Xu, *Chem. Soc. Rev.* **2020**, *49*, 1414–1448.
[5] W. Hao, R. Wu, H. Huang, X. Ou, L. Wang, D. Sun, X. Ma, Y. Guo, *Energy Environ. Sci.* **2020**, *13*, 102–110.
[6] D. Zhao, Z. Zhuang, X. Cao, C. Zhang, Q. Peng, C. Chen, Y. Li, *Chem. Soc. Rev.* **2020**, *49*, 2215–2264.
[7] G. Singh, J. Lee, A. Karakoti, R. Bahadur, J. Yi, D. Zhao, K. AlBahily, A. Vinu, *Chem. Soc. Rev.* **2020**, *49*, 4360–4404.
[8] R. B. Song, W. Zhu, J. Fu, Y. Chen, L. Liu, J. R. Zhang, Y. Lin, J. J. Zhu, *Adv. Mater.* **2019**, *32*, 1903796.
[9] Y. Lu, J. Zhang, W. Wei, D. D. Ma, X. T. Wu, Q.-L. Zhu, *ACS Appl. Mater. Interfaces* **2020**, *12*, 37986–37992.
[10] Z. Zhang, C. Ma, Y. Tu, R. Si, J. Wei, S. Zhang, Z. Wang, J.-F. Li, Y. Wang, D. Deng, *Nano Res.* **2019**, *12*, 2313–2317.
[11] P. Lamagni, M. Miola, J. Catalano, M. S. Hvid, M. A. H. Mamakhel, M. Christensen, M. R. Madsen, H. S. Jeppesen, X. M. Hu, K. Daasbjerg, T. Skrydstrup, N. Lock, *Adv. Funct. Mater.* **2020**, *30*, 1910408.
[12] M. Li, H. Wang, W. Luo, P. C. Sherrell, J. Chen, J. Yang, *Adv. Mater.* **2020**, *32*, 2001848.
[13] W. Guo, K. Zhang, Z. Liang, R. Zou, Q. Xu, *Chem. Soc. Rev.* **2019**, *48*, 5658–5716.
[14] S. Zhao, X. Lu, L. Wang, J. Gale, R. Amal, *Adv. Mater.* **2019**, *31*, 1805367.
[15] Q. Wang, Y. Lei, D. Wang, Y. Li, *Energy Environ. Sci.* **2019**, *12*, 1730–1750.
[16] R. Zhao, H. Xie, L. Chang, X. Zhang, X. Zhu, X. Tong, T. Wang, Y. Luo, P. Wei, Z. Wang, X. Sun, *EnergyChem* **2019**, *1*, 100011.
[17] X. L. Ma, J. C. Liu, H. Xiao, J. Li, *J. Am. Chem. Soc.* **2018**, *140*, 46–49.
[18] M. Kuang, W. Huang, C. Hegde, W. Fang, X. Tan, C. Liu, J. Ma, Q. Yan, *Mater. Horiz.* **2020**, *7*, 32–53.
[19] L. Kong, M. Zhong, W. Shuang, Y. Xu, X. H. Bu, *Chem. Soc. Rev.* **2020**, *49*, 2378–2407.
[20] Y. Guo, T. Park, J. W. Yi, J. Henzie, J. Kim, Z. Wang, B. Jiang, Y. Bando, Y. Sugahara, J. Tang, Y. Yamauchi, *Adv. Mater.* **2019**, *31*, 1807134.
[21] W. Li, S. Xue, S. Watzele, S. Hou, J. Fichtner, A. L. Semrau, L. Zhou, A. Welle, A. S. Bandarenka, R. A. Fischer, *Angew. Chem. Int. Ed.* **2020**, *59*, 5837–5843; *Angew. Chem.* **2020**, *132*, 5886–5892.
[22] Z. P. Wu, X. F. Lu, S. Q. Zang, X. W. Lou, *Adv. Funct. Mater.* **2020**, *30*, 1910274.
[23] S. Anantharaj, S. Noda, *Small* **2020**, *16*, 1905779.
[24] L. Li, J. He, Y. Wang, X. Lv, X. Gu, P. Dai, D. Liu, X. Zhao, *J. Mater. Chem. A* **2019**, *7*, 1964–1988.
[25] T. Schuler, T. Kimura, T. J. Schmidt, F. N. Büchi, *Energy Environ. Sci.* **2020**, *13*, 2153–2166.
[26] C. Li, Q. Li, Y. V. Kaneti, D. Hou, Y. Yamauchi, Y. Mai, *Chem. Soc. Rev.* **2020**, *49*, 4681–4736.
[27] S. Ren, Q. Yu, X. Yu, P. Rong, L. Jiang, J. Jiang, *Sci. China Mater.* **2020**, *63*, 903–920.
[28] C. F. Wen, F. Mao, Y. Liu, X. Y. Zhang, H. Q. Fu, L. R. Zheng, P. F. Liu, H. G. Yang, *ACS Catal.* **2019**, *10*, 1086–1093.
[29] Z. Lu, B. Wang, Y. Hu, W. Liu, Y. Zhao, R. Yang, Z. Li, J. Luo, B. Chi, Z. Jiang, M. Li, S. Mu, S. Liao, J. Zhang, X. Sun, *Angew. Chem. Int. Ed.* **2019**, *58*, 2622–2626; *Angew. Chem.* **2019**, *131*, 2648–2652.
[30] D. Zhang, W. Chen, Z. Li, Y. Chen, L. Zheng, Y. Gong, Q. Li, R. Shen, Y. Han, W. C. Cheong, L. Gu, Y. Li, *Chem. Commun.* **2018**, *54*, 4274–4277.
[31] L. Zhang, J. Fischer, Y. Jia, X. Yan, W. Xu, X. Wang, J. Chen, D. Yang, H. Liu, L. Zhuang, M. Hankel, D. J. Searles, K. Huang, S. Feng, C. L. Brown, X. Yao, *J. Am. Chem. Soc.* **2018**, *140*, 10757–10763.
[32] T. Sun, L. Xu, D. Wang, Y. Li, *Nano Res.* **2019**, *12*, 2067–2080.
[33] C. Zhu, Q. Shi, S. Feng, D. Du, Y. Lin, *ACS Energy Lett.* **2018**, *3*, 1713–1721.
[34] Z. Li, S. Ji, Y. Liu, X. Cao, S. Tian, Y. Chen, Z. Niu, Y. Li, *Chem. Rev.* **2019**, *120*, 623–682.
[35] A. Alarawi, V. Ramalingam, J.-H. He, *Mater. Today* **2019**, *11*, 1–23.
[36] S. Ji, Y. Chen, X. Wang, Z. Zhang, D. Wang, Y. Li, *Chem. Rev.* **2020**, DOI: 10.1021/acs.chemrev.1029b00818.
[37] N. Wang, Q. Sun, J. Yu, *Adv. Mater.* **2019**, *31*, 1803966.
[38] G. Yilmaz, S. B. Peh, D. Zhao, G. W. Ho, *Adv. Sci.* **2019**, *6*, 1901129.
[39] Y. S. Wei, M. Zhang, R. Zou, Q. Xu, *Chem. Rev.* **2020**, DOI: 10.1021/acs.chemrev.1029b00757.
[40] H. Huang, K. Shen, F. Chen, Y. Li, *ACS Catal.* **2020**, *10*, 6579–6586.
[41] Y. Zheng, S.-Z. Qiao, *Natl. Sci. Rev.* **2018**, *5*, 626–627.
[42] J. Li, S. Chen, N. Yang, M. Deng, S. Ibraheem, J. Deng, J. Li, L. Li, Z. Wei, *Angew. Chem. Int. Ed.* **2019**, *58*, 7035–7039; *Angew. Chem.* **2019**, *131*, 7109–7113.
[43] J. Zhang, Q.-a. Huang, J. Wang, J. Wang, J. Zhang, Y. Zhao, *Chin. J. Catal.* **2020**, *41*, 783–798.
[44] Z. Liang, C. Qu, D. Xia, R. Zou, Q. Xu, *Angew. Chem. Int. Ed.* **2018**, *57*, 9604–9633; *Angew. Chem.* **2018**, *130*, 9750–9780.
[45] A. Han, B. Wang, A. Kumar, Y. Qin, J. Jin, X. Wang, C. Yang, B. Dong, Y. Jia, J. Liu, X. Sun, *Small Methods* **2019**, *3*, 1800471.
[46] L. Jiao, H.-L. Jiang, *Chem* **2019**, *5*, 786–804.

[47] D. Ma, Q.-L. Zhu, *Coord. Chem. Rev.* **2020**, *422*, 213483.
[48] B. Qiao, A. Wang, X. Yang, L. F. Allard, Z. Jiang, Y. Cui, J. Liu, J. Li, T. Zhang, *Nat. Chem.* **2011**, *3*, 634–641.
[49] L. Fan, P. F. Liu, X. Yan, L. Gu, Z. Z. Yang, H. G. Yang, S. Qiu, X. Yao, *Nat. Commun.* **2016**, *7*, 10667.
[50] P. Yin, T. Yao, Y. Wu, L. Zheng, Y. Lin, W. Liu, H. Ju, J. Zhu, X. Hong, Z. Deng, G. Zhou, S. Wei, Y. Li, *Angew. Chem. Int. Ed.* **2016**, *55*, 10800–10805; *Angew. Chem.* **2016**, *128*, 10958–10963.
[51] C. Zhao, X. Dai, T. Yao, W. Chen, X. Wang, J. Wang, J. Yang, S. Wei, Y. Wu, Y. Li, *J. Am. Chem. Soc.* **2017**, *139*, 8078–8081.
[52] Z. Geng, Y. Liu, X. Kong, P. Li, K. Li, Z. Liu, J. Du, M. Shu, R. Si, J. Zeng, *Adv. Mater.* **2018**, *30*, 1803498.
[53] M. Liu, L. Wang, K. Zhao, S. Shi, Q. Shao, L. Zhang, X. Sun, Y. Zhao, J. Zhang, *Energy Environ. Sci.* **2019**, *12*, 2890–2923.
[54] U. Martinez, S. Komini Babu, E. F. Holby, H. T. Chung, X. Yin, P. Zelenay, *Adv. Mater.* **2019**, *31*, 1806545.
[55] X. F. Lu, B. Y. Xia, S. Q. Zang, X. W. D. Lou, *Angew. Chem. Int. Ed.* **2020**, *59*, 4634–4650; *Angew. Chem.* **2020**, *132*, 4662–4678.
[56] C. X. Zhao, B. Q. Li, J. N. Liu, Q. Zhang, *Angew. Chem. Int. Ed.* **2020**, DOI: 10.1002/anie.202003917; *Angew. Chem.* **2020**, DOI: 10.1002/ange.202003917.
[57] X. Chen, D.-D. Ma, B. Chen, K. Zhang, R. Zou, X.-T. Wu, Q.-L. Zhu, *Appl. Catal. B* **2020**, *267*, 118720.
[58] Y. Deng, B. Chi, X. Tian, Z. Cui, E. Liu, Q. Jia, W. Fan, G. Wang, D. Dang, M. Li, K. Zang, J. Luo, Y. Hu, S. Liao, X. Sun, S. Mukerjee, *J. Mater. Chem. A* **2019**, *7*, 5020–5030.
[59] J.-D. Yi, R. Xu, Q. Wu, T. Zhang, K.-T. Zang, J. Luo, Y.-L. Liang, Y.-B. Huang, R. Cao, *ACS Energy Lett.* **2018**, *3*, 883–889.
[60] H. Zhang, S. Ding, S. Hwang, X. Zhao, D. Su, H. Xu, H. Yang, G. Wu, *J. Electrochem. Soc.* **2019**, *166*, F3116-F3122.
[61] T. Al-Zoubi, Y. Zhou, X. Yin, B. Janicek, C. Sun, C. E. Schulz, X. Zhang, A. A. Gewirth, P. Huang, P. Zelenay, H. Yang, *J. Am. Chem. Soc.* **2020**, *142*, 5477–5481.
[62] J. Wang, G. Han, L. Wang, L. Du, G. Chen, Y. Gao, Y. Ma, C. Du, X. Cheng, P. Zuo, G. Yin, *Small* **2018**, *14*, 1704282.
[63] Q.-L. Zhu, W. Xia, L.-R. Zheng, R. Zou, Z. Liu, Q. Xu, *ACS Energy Lett.* **2017**, *2*, 504–511.
[64] H. Zhang, S. Hwang, M. Wang, Z. Feng, S. Karakalos, L. Luo, Z. Qiao, X. Xie, C. Wang, D. Su, Y. Shao, G. Wu, *J. Am. Chem. Soc.* **2017**, *139*, 14143–14149.
[65] R. Jiang, L. Li, T. Sheng, G. Hu, Y. Chen, L. Wang, *J. Am. Chem. Soc.* **2018**, *140*, 11594–11598.
[66] Y. Deng, B. Chi, J. Li, G. Wang, L. Zheng, X. Shi, Z. Cui, L. Du, S. Liao, K. Zang, J. Luo, Y. Hu, X. Sun, *Adv. Energy Mater.* **2019**, *9*, 1802856.
[67] Y. Chen, S. Ji, Y. Wang, J. Dong, W. Chen, Z. Li, R. Shen, L. Zheng, Z. Zhuang, D. Wang, Y. Li, *Angew. Chem. Int. Ed.* **2017**, *56*, 6937–6941; *Angew. Chem.* **2017**, *129*, 7041–7045.
[68] X. Chen, N. Wang, K. Shen, Y. Xie, Y. Tan, Y. Li, *ACS Appl. Mater. Interfaces* **2019**, *11*, 25976–25985.
[69] X. Zhang, X. Han, Z. Jiang, J. Xu, L. Chen, Y. Xue, A. Nie, Z. Xie, Q. Kuang, L. Zheng, *Nano Energy* **2020**, *71*, 104547.
[70] C. C. Hou, L. Zou, L. Sun, K. Zhang, Z. Liu, Y. Li, C. Li, R. Zou, J. Yu, Q. Xu, *Angew. Chem. Int. Ed.* **2020**, *59*, 7384–7389; *Angew. Chem.* **2020**, *132*, 7454–7459.
[71] Y. Chen, S. Ji, S. Zhao, W. Chen, J. Dong, W. C. Cheong, R. Shen, X. Wen, L. Zheng, A. I. Rykov, S. Cai, H. Tang, Z. Zhuang, C. Chen, Q. Peng, D. Wang, Y. Li, *Nat. Commun.* **2018**, *9*, 5422.
[72] L. Jiao, G. Wan, R. Zhang, H. Zhou, S.-H. Yu, H.-L. Jiang, *Angew. Chem. Int. Ed.* **2018**, *57*, 8525–8529; *Angew. Chem.* **2018**, *130*, 8661–8665.
[73] D. L. Meng, C. H. Chen, J. D. Yi, Q. Wu, J. Liang, Y. B. Huang, R. Cao, *Research* **2019**, *2019*, 1768595.
[74] Y. Hao, Y. Xu, W. Liu, X. Sun, *Mater. Horiz.* **2018**, *5*, 108–115.
[75] H. Ge, G. Li, J. Shen, W. Ma, X. Meng, L. Xu, *Appl. Catal. B* **2020**, *275*, 119104.
[76] Y. Jiang, Y.-P. Deng, J. Fu, D. U. Lee, R. Liang, Z. P. Cano, Y. Liu, Z. Bai, S. Hwang, L. Yang, D. Su, W. Chu, Z. Chen, *Adv. Energy Mater.* **2018**, *8*, 1702900.
[77] J.-Y. Zhao, R. Wang, S. Wang, Y.-R. Lv, H. Xu, S.-Q. Zang, *J. Mater. Chem. A* **2019**, *7*, 7389–7395.
[78] X. Han, X. Ling, Y. Wang, T. Ma, C. Zhong, W. Hu, Y. Deng, *Angew. Chem. Int. Ed.* **2019**, *58*, 5359–5364; *Angew. Chem.* **2019**, *131*, 5413–5418.
[79] T. Wang, Z. Kou, S. Mu, J. Liu, D. He, I. S. Amiinu, W. Meng, K. Zhou, Z. Luo, S. Chaemchuen, F. Verpoort, *Adv. Funct. Mater.* **2018**, *28*, 1705048.
[80] W. Sun, L. Du, Q. Tan, J. Zhou, Y. Hu, C. Du, Y. Gao, G. Yin, *ACS Appl. Mater. Interfaces* **2019**, *11*, 41258–41266.
[81] X. X. Wang, D. A. Cullen, Y.-T. Pan, S. Hwang, M. Wang, Z. Feng, J. Wang, M. H. Engelhard, H. Zhang, Y. He, Y. Shao, D. Su, K. L. More, J. S. Spendelow, G. Wu, *Adv. Mater.* **2018**, *30*, 1706758.
[82] Y. He, S. Hwang, D. A. Cullen, M. A. Uddin, L. Langhorst, B. Li, S. Karakalos, A. J. Kropf, E. C. Wegener, J. Sokolowski, M. Chen, D. Myers, D. Su, K. L. More, G. Wang, S. Litster, G. Wu, *Energy Environ. Sci.* **2019**, *12*, 250–260.
[83] Y. Xiong, W. Sun, P. Xin, W. Chen, X. Zheng, W. Yan, L. Zheng, J. Dong, J. Zhang, D. Wang, Y. Li, *Adv. Mater.* **2020**, *32*, 2000896.
[84] Y. Qu, Z. Li, W. Chen, Y. Lin, T. Yuan, Z. Yang, C. Zhao, J. Wang, C. Zhao, X. Wang, F. Zhou, Z. Zhuang, Y. Wu, Y. Li, *Nat. Catal.* **2018**, *1*, 781–786.
[85] J. Li, M. Chen, D. A. Cullen, S. Hwang, M. Wang, B. Li, K. Liu, S. Karakalos, M. Lucero, H. Zhang, C. Lei, H. Xu, G. E. Sterbinsky, Z. Feng, D. Su, K. L. More, G. Wang, Z. Wang, G. Wu, *Nat. Catal.* **2018**, *1*, 935–945.
[86] H. Zhang, A. W. Maijenburg, X. Li, S. L. Schweizer, R. B. Wehrspohn, *Adv. Funct. Mater.* **2020**, 2003261.
[87] J. Zhou, J. Cheng, B. Wang, H. Peng, J. Lu, *Energy Environ. Sci.* **2020**, *13*, 1933–1970.
[88] Q. Zha, F. Yuan, G. Qin, Y. Ni, *Inorg. Chem.* **2020**, *59*, 1295–1305.
[89] X. Song, S. Chen, L. Guo, Y. Sun, X. Li, X. Cao, Z. Wang, J. Sun, C. Lin, Y. Wang, *Adv. Energy Mater.* **2018**, *8*, 1801101.
[90] L. Tao, C.-Y. Lin, S. Dou, S. Feng, D. Chen, D. Liu, J. Huo, Z. Xia, S. Wang, *Nano Energy* **2017**, *41*, 417–425.
[91] S. Dou, C. L. Dong, Z. Hu, Y. C. Huang, J. L. Chen, L. Tao, D. Yan, D. Chen, S. Shen, S. Chou, S. Wang, *Adv. Funct. Mater.* **2017**, *27*, 1702546.
[92] W. Zang, A. Sumboja, Y. Ma, H. Zhang, Y. Wu, S. Wu, H. Wu, Z. Liu, C. Guan, J. Wang, S. J. Pennycook, *ACS Catal.* **2018**, *8*, 8961–8969.
[93] Y. Pan, C. Zhang, Y. Lin, Z. Liu, M. Wang, C. Chen, *Sci. China Mater.* **2020**, *63*, 921–948.
[94] D.-H. He, J.-J. Liu, Y. Wang, F. Li, B. Li, J.-B. He, *Electrochim. Acta* **2019**, *308*, 285–294.
[95] Y. Ji, H. Dong, C. Liu, Y. Li, *Nanoscale* **2019**, *11*, 454–458.
[96] H. Wang, W. Fu, X. Yang, Z. Huang, J. Li, H. Zhang, Y. Wang, *J. Mater. Chem. A* **2020**, *8*, 6926–6956.
[97] W. Zhao, G. Wan, C. Peng, H. Sheng, J. Wen, H. Chen, *ChemSusChem* **2018**, *11*, 3473–3479.
[98] J. Chen, B. Ren, H. Cui, C. Wang, *Small* **2020**, *16*, 1907556.
[99] S. Xu, S. Gong, H. Jiang, P. Shi, J. Fan, Q. Xu, Y. Min, *Appl. Catal. B* **2020**, *267*, 118661.
[100] P. V. Sarma, A. Kayal, C. H. Sharma, M. Thalakulam, J. Mitra, M. M. Shaijumon, *ACS Nano* **2019**, *13*, 10448–10455.
[101] W. Chen, J. Pei, C. T. He, J. Wan, H. Ren, Y. Wang, J. Dong, K. Wu, W. C. Cheong, J. Mao, X. Zheng, W. Yan, Z. Zhuang, C. Chen, Q. Peng, D. Wang, Y. Li, *Adv. Mater.* **2018**, *30*, 1800396.
[102] F. Pan, Y. Yang, *Energy Environ. Sci.* **2020**, *13*, 2275–2309.
[103] Q. Cui, G. Qin, W. Wang, K. R. Geethalakshmi, A. Du, Q. Sun, *Appl. Surf. Sci.* **2020**, *500*, 143993.
[104] D.-D. Ma, S.-G. Han, C. Cao, X. Li, X.-T. Wu, Q.-L. Zhu, *Appl. Catal. B* **2020**, *264*, 118530.
[105] X. Wang, Z. Chen, X. Zhao, T. Yao, W. Chen, R. You, C. Zhao, G. Wu, J. Wang, W. Huang, J. Yang, X. Hong, S. Wei, Y. Wu, Y. Li, *Angew. Chem. Int. Ed.* **2018**, *57*, 1944–1948; *Angew. Chem.* **2018**, *130*, 1962–1966.
[106] Y.-N. Gong, L. Jiao, Y. Qian, C.-Y. Pan, L. Zheng, X. Cai, B. Liu, S.-H. Yu, H.-L. Jiang, *Angew. Chem. Int. Ed.* **2020**, *59*, 2705–2709; *Angew. Chem.* **2020**, *132*, 2727–2731.
[107] F. Pan, H. Zhang, K. Liu, D. Cullen, K. More, M. Wang, Z. Feng, G. Wang, G. Wu, Y. Li, *ACS Catal.* **2018**, *8*, 3116–3122.
[108] C. Cao, D. D. Ma, J. F. Gu, X. Xie, G. Zeng, X. Li, S. G. Han, Q. L. Zhu, X. T. Wu, Q. Xu, *Angew. Chem. Int. Ed.* **2020**, *132*, 15014–15020; *Angew. Chem.* **2020**, *132*, 15124–15130.
[109] E. Zhang, T. Wang, K. Yu, J. Liu, W. Chen, A. Li, H. Rong, R. Lin, S. Ji, X. Zheng, Y. Wang, L. Zheng, C. Chen, D. Wang, J. Zhang, Y. Li, *J. Am. Chem. Soc.* **2019**, *141*, 16569–16573.
[110] X. Li, Q.-L. Zhu, *EnergyChem* **2020**, *2*, 100033.
[111] G. F. Chen, S. Ren, L. Zhang, H. Cheng, Y. Luo, K. Zhu, L. X. Ding, H. Wang, *Small Methods* **2018**, *3*, 1800337.
[112] S. L. Foster, S. I. P. Bakovic, R. D. Duda, S. Maheshwari, R. D. Milton, S. D. Minteer, M. J. Janik, J. N. Renner, L. F. Greenlee, *Nat. Can.* **2018**, *1*, 490–500.
[113] B. H. R. Suryanto, H.-L. Du, D. Wang, J. Chen, A. N. Simonov, D. R. MacFarlane, *Nat. Can.* **2019**, *2*, 290–296.
[114] Z. Yan, M. Ji, J. Xia, H. Zhu, *Adv. Energy Mater.* **2019**, *10*, 1902020.

[115] R. Zhang, L. Jiao, W. Yang, G. Wan, H.-L. Jiang, *J. Mater. Chem. A* **2019**, *7*, 26371–26377.
[116] C. Tang, S. Z. Qiao, *Chem. Soc. Rev.* **2019**, *48*, 3166–3180.
[117] L. Shi, Y. Yin, S. Wang, X. Xu, H. Wu, J. Zhang, S. Wang, H. Sun, *Appl. Catal. B* **2020**, *278*, 119325.
[118] D. Liu, B. Wang, H. Li, S. Huang, M. Liu, J. Wang, Q. Wang, J. Zhang, Y. Zhao, *Nano Energy* **2019**, *58*, 277–283.
[119] R. Zhao, Z. Liang, S. Gao, C. Yang, B. Zhu, J. Zhao, C. Qu, R. Zou, Q. Xu, *Angew. Chem. Int. Ed.* **2019**, *58*, 1975–1979; *Angew. Chem.* **2019**, *131*, 1997–2001.
[120] M. Kuang, Q. Wang, P. Han, G. Zheng, *Adv. Energy Mater.* **2017**, *7*, 1700193.
[121] J. Jiao, R. Lin, S. Liu, W. C. Cheong, C. Zhang, Z. Chen, Y. Pan, J. Tang, K. Wu, S. F. Hung, H. M. Chen, L. Zheng, Q. Lu, X. Yang, B. Xu, H. Xiao, J. Li, D. Wang, Q. Peng, C. Chen, Y. Li, *Nat. Chem.* **2019**, *11*, 222–228.
[122] L. Zheng, S. Yu, X. Lu, W. Fan, B. Chi, Y. Ye, X. Shi, J. Zeng, X. Li, S. Liao, *ACS Appl. Mater. Interfaces* **2020**, *12*, 13878–13887.
[123] M. Xiao, H. Zhang, Y. Chen, J. Zhu, L. Gao, Z. Jin, J. Ge, Z. Jiang, S. Chen, C. Liu, W. Xing, *Nano Energy* **2018**, *46*, 396–403.
[124] Z. Li, H. He, H. Cao, S. Sun, W. Diao, D. Gao, P. Lu, S. Zhang, Z. Guo, M. Li, R. Liu, D. Ren, C. Liu, Y. Zhang, Z. Yang, J. Jiang, G. Zhang, *Appl. Catal. B* **2019**, *240*, 112–121.
[125] J. Wang, Z. Huang, W. Liu, C. Chang, H. Tang, Z. Li, W. Chen, C. Jia, T. Yao, S. Wei, Y. Wu, Y. Li, *J. Am. Chem. Soc.* **2017**, *139*, 17281–17284.
[126] J. Wang, W. Liu, G. Luo, Z. Li, C. Zhao, H. Zhang, M. Zhu, Q. Xu, X. Wang, C. Zhao, Y. Qu, Z. Yang, T. Yao, Y. Li, Y. Lin, Y. Wu, Y. Li, *Energy Environ. Sci.* **2018**, *11*, 3375–3379.
[127] W. Ren, X. Tan, W. Yang, C. Jia, S. Xu, K. Wang, S. C. Smith, C. Zhao, *Angew. Chem. Int. Ed.* **2019**, *58*, 6972–6976; *Angew. Chem.* **2019**, *131*, 7046–7050.

Manuscript received: September 3, 2020
Revised manuscript received: October 20, 2020
Accepted manuscript online: October 22, 2020
Version of record online: October 29, 2020